ELECTRONIC SUPPLEMENTARY INFORMATION

FOR

UV-Photoelectron spectroscopy of stable radicals: The electronic structure of planar Blatter radicals as materials for organic electronics

Aniket A. Hande,[a] Clovis Darrigan,[a] Paulina Bartos,[b] Patrick Baylère,[a] Anna Pietrzak,[c,d] Piotr Kaszyński,[b,d,e*] and Anna Chrostowska[a*]

Table of Context

1. Synthetic details and characterization …S2
2. NMR spectra …S7
3. XRD data collection, refinement and structure information …S12
4. Electronic absorption spectroscopy …S15
5. Ultraviolet photoelectron spectra …S21
6. Electrochemical data …S23
7. EPR spectroscopy …S25
8. Correlation analysis of literature experimental data …S28
9. Computational details and results …S31
    a) General …S31
    b) Molecular geometry …S31
    c) Ionization energies (IE_n) …S32
    d) Electron Affinities (EA) …S43
    e) Excitation energies …S43
    f) Isotropic Fermi constants (A^{FC}) …S45
    g) Spin delocalization …S49
    h) Atomic coordinates for CAM-B3LYP/6-311G(d,p) optimized geometry and total energy …S52
10. References …S57

1. Synthetic details and characterization

Table S1. Synthesis of radicals **1** and summary of yields. [a]

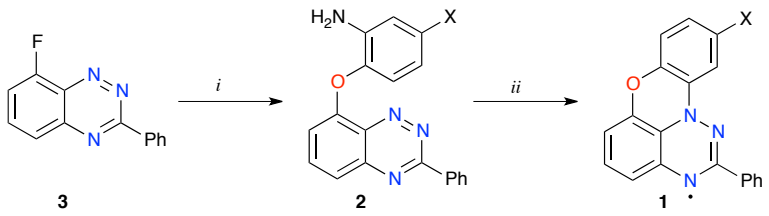

Compound	X	Yields (%)	
		2	**1**
a [b]	H	78%	57-64%
b	F	50%	45%
c	Cl	53%	55%
d	Br	52%	18%
e [b]	CN	80%	68%
f	CF_3	48%	62%
g	OMe	55%	52%

[a] Reagents and conditions: *i*) subst. *o*-aminophenol, 60% NaH, DMSO, 100 °C, 1 h; *ii*) *t*-BuONO, PhCl, rt, 15 min, 70 °C, 45 min. [b] Ref [1].

General. Commercial reagents and solvents were purchased from MERCK, Aldrich. Heat for reaction requiring elevated temperatures was supplied using oil baths. NMR spectra were obtained at 600 MHz (^{1}H), 151 MHz (^{13}C) in DMSO-d_6 and referenced to the solvent (δ = 2.50 ppm for ^{1}H and δ = 39.52 ppm for ^{13}C) for all no-radicals. IR spectra were recorded using Nexus FT-IR Thermo Nicolet IR spectrometer in KBr tablets. Melting points were determined on a Stuart SMP30 Advanced Digital Melting Point Apparatus and are uncorrected. High-resolution mass spectrometry (HRMS) measurements were performed using SYNAPT G2-Si High Definition Mass Spectrometry equipped with an ESI or APCI source and Quantitative Time-of-Flight (QuanTof) mass analyzer. In all cases little or no fragmentation is observed and the M or M+H peaks are the most intense signals. Preparation of radicals **1a** and **1e** was reported earlier.[1]

General procedure for synthesis of radicals with Diazotization of amines 2 with *t*-BuONO.[1] Under an atmosphere of Ar, amine 2 (0.25 mmol) was dissolved in dry PhCl (3 mL), *t*-BuONO (0.75 mmol, 3 eq.) was added dropwise with stirring, gradually heated to 70 °C over a period of 15 min and the temperature of 70 °C was maintained for 45 min. After 1 h TLC analysis showed that the substrate was no longer present. The reaction mixture was cooled, SiO_2 (passivated with 2% solution of Et_3N in CH_2Cl_2) was added and the solvent was evaporated (< 40 ºC). The resulting solid was deposited on the top of a passivated silica gel plug and the product eluted with 20% AcOEt/pet. ether mixture. The isolated product was recrystallized by slow evaporation of a CH_2Cl_2 / cyclohexane solution.

10-Fluoro-2-phenyl-3H-[1,2,4]triazino[5,6,1-kl]phenoxazin-3-yl (1b). Eluent: pet. ether/AcOEt, 9:1; 45 % yield. Fine green crystals: mp 180 °C. (MeCN); IR (KBr) *n* 1611, 1502, 1448, 1385, 1245, 1116, 787, 686 cm^{-1}; UV (CH2Cl2) λ_{max} (log ε) 259(4.42), 292(4.43), 370 (3.76), 481 (3.45), 583(3.31), 634(3.36), 694(3.25) nm; HRMS (ESI-TOF) $[M+H]^+$ *m/z* calcd for C19H12FN3O: 317.0964; found: 317.0976. Anal. Calcd for $C_{19}H11FN3O$: C, 72.15; H, 3.51; N, 13.28. Found C, 72.20; H, 3.72; N, 13.22.

10-Chloro-2-phenyl-3*H*-[1,2,4]triazino[5,6,1-*kl*]phenoxazin-3-yl (1c). Eluent: pet. ether/AcOEt, 9:1; 55 % yield. Green crystals: mp 201-202 °C. (MeCN); IR (KBr) *v* 1600, 1462, 1386, 1272, 1125, 867, 788, 696 cm^{-1}; UV (CH_2Cl_2) λ_{max} (*log* ε) 262 (4.49), 287 (4.44), 365 (3.80), 481 (3.45), 585 (3.30), 626 (3.35), 689 (3.24) nm; HRMS (ESI-TOF) $[M+H]^+$ *m/z* calcd for $C_{19}H_{12}ClN_3O$: 333.0669; found: 333.0674. Anal. Calcd for $C_{19}H_{11}ClN_3O$: C, 68.58; H, 3.33; N, 12.63. Found C, 68.54; H, 3.56; N, 12.60.

10-Bromo-2-phenyl-3*H*-[1,2,4]triazino[5,6,1-*kl*]phenoxazin-3-yl (1d). Eluent: pet. ether/AcOEt, 9:1; 18 % yield. Blue-green crystals: mp 210-211 °C. (MeCN); IR (KBr) *v* 1723, 1461, 1269, 1117, 788, 731, 696 cm^{-1}; UV (CH_2Cl_2) λ_{max} (*log* ε) 260 (4.20), 288 (4.15), 369 (3.40), 476 (2.99), 578 (2.79), 625 (2.82), 679 (2.68) nm; HRMS (ESI-TOF) $[M+H]^+$ *m/z* calcd for $C_{19}H_{12}BrN_3O$: 377.0164; found: 377.0166. Anal. Calcd for $C_{19}H_{11}BrN_3O$: C, 60.50; H, 2.94; N, 11.14. Found C, 60.42; H, 3.07; N, 11.12.

10-Trifluoromethyl-2-phenyl-3*H*-[1,2,4]triazino[5,6,1-*kl*]phenoxazin-3-yl (1f). Eluent: pet. ether/AcOEt, 9:1; 62% yield; green crystals: mp 164-166 °C. (MeCN); IR (KBr) *v* 1564, 1507,

1445, 1387, 1329, 1271, 1124, 780, 694 cm^{-1}; UV (CH_2Cl_2) λ_{max} (*log* ε) 261 (4.46), 280 (4.43), 356 (3.67), 477 (3.15), 572 (2.97), 611 (3.00), 677 (2.87) nm; HRMS (ESI-TOF) $[M]^+$ *m/z* calcd for $C_{20}H_{11}F_3N_3O$: 366.0854; found: 366.0872. Anal. Calcd for $C_{20}H_{11}F_3N_3O$: C, 65.58; H, 3.03; N, 11.47. Found C, 65.32; H, 3.34; N, 11.45.

10-Methoxy-2-phenyl-3H-[1,2,4]triazino[5,6,1-kl]phenoxazin-3-yl (1g). Eluent: pet. ether/AcOEt, 8:2; 52% yield; brown crystals: mp 164-166 °C. (MeCN); IR (KBr) ν 1613, 1503, 1462, 1385, 1257, 1202, 1032, 788, 691 cm^{-1}; UV (CH_2Cl_2) λ_{max} (log ε) 239 (4.42), 264 (4.38), 292 (4.32), 305 (4.30), 324sh (4.17), 347sh (3.89), 483 (3.34), 602sh (3.30), 645 (3.41), 709 (3.34) nm; HRMS (ESI-TOF) $[M+H]^+$ *m/z* calcd for $C_{20}H_{15}N_3O_2$: 329.1164; found: 329.1159. Anal. Calcd for $C_{20}H_{14}N_3O_2$: C, 73.16; H, 4.30; N, 12.80. Found C, 73.13; H, 4.55; N, 12.62.

General method for preparation of 8-(*ortho*-amioaryloxy)-3-phenylbenzo[*e*][1,2,4]triazine (2).[1] To a stirred solution of an appropriate *ortho*-aminophenol (2.20 mmol) in DMSO (8 mL) 60% NaH (90 mg, 2.20 mmol) was added in one portion. After 15 min 8-fluoro-3-phenylbenzo[*e*][1,2,4]triazine[2] (**3**, 450.4 mg, 2.00 mmol) was added and the reaction was stirred under Ar at 100 ºC for 1 h. After cooling, CH_2Cl_2 (50 mL) was added and organic layer was washed well with water (3x50 mL) and brine (50 mL). The combined organic extracts were dried (Na_2SO_4) and the solvent was evaporated. The resulting solid residue was adsorbed onto passivated silica gel and was purified by column chromatography (passivated silica), solvent was evaporated and the resulting amine **2** was recrystallized (MeCN).

8-(2-Amino-4-fluoro-1-phenyloxy)-3-phenylbenzo[e][1,2,4]triazine (2b). Eluent: pet. ether/AcOEt, 10:2; 400 mg (50% yield) yellow crystals: mp 234 °C (MeCN); ^{1}H NMR (600 MHz, DMSO-d_6) ^{1}H NMR (600 MHz, DMSO) δ 5.47 (s, 2H), 6.41 (td, J_1 = 8.5 Hz, J_2 = 3.0 Hz, 1H), 6.67 (dd, J_1 = 10.9 Hz, J_2 = 3.1 Hz, 1H), 6.92 (dd, J_1 = 7.9 Hz, J_2 = 1.0 Hz, 1H), 7.10 (d, J_1 = 8.7 Hz, J_2 = 5.6 Hz, 1H), 7.65 – 7.70 (m, 3H), 7.76 (dd, J_1 = 8.5 Hz, J_2 = 1 .0 Hz, 1H), 7.79 (t, *J* = 8.2 Hz, 1H), 8.65 – 8.70 (m, 2H); ^{13}C NMR (151 MHz, $CDCl_3$) δ 101.9 (d, *J* = 26.5 Hz), 102.2 (d, *J* = 23.8 Hz), 112.3, 121.3, 122.8 (d, *J* = 10.9 Hz), 128.3, 129.3, 131.8, 135.1, 136.3 (d, *J* = 1.7 Hz), 137.3, 139.6, 141.3, 142.5 (d, *J* = 12.1 Hz), 154.4, 158.9, 160.5 (d, *J* = 238.3 Hz); IR (KBr) *v* 3250 and 3192 (N-H), 1614, 1566, 1500, 1198, 1175, 854, 786, 698 cm^{-1}; HRMS (ESI-TOF) $[M+H]^+$ *m/z* calcd for

$C_{19}H_{14}FN_4O$: 333.1152; found: 333.1169. Anal. Calcd for $C_{19}H_{13}FN_4O$: C, 68.67; H, 3.94; N, 16.86. Found C, 68.55; H, 4.11; N, 16.85.

8-(2-Amino-4-chloro-1-phenyloxy)-3-phenylbenzo[e][1,2,4]triazine (2c). Eluent: pet. ether/AcOEt, 10:2; 490 mg (53% yield) yellow crystals: mp 240 °C (MeCN); ^{1}H NMR (600 MHz, DMSO-d_6) δ 5.50 (s, 2H), 6.62 (dd, J_1 = 8.4 Hz, J_2 = 2.5 Hz, 1H), 6.92 (d, J = 2.5 Hz, 1H), 6.99 (d, J = 7.7 Hz, 1H), 7.06 (d, J = 8.4 Hz, 1H), 7.65–7.70 (m, 3H), 7.79 (d, J = 8.2 Hz, 1H), 8.00 (t, J = 8.2 Hz, 1H), 8.65–8.70 (m, 2H); ^{13}C NMR (151 MHz, DMSO-d_6) δ 113.4, 115.5, 116.0, 122.1, 123.2, 128.8, 129.7, 130.5, 132.3, 135.6, 137.7, 139.7, 140.0, 141.8, 142.7, 154.4, 159.4; IR (KBr) v 3292 and 3198 (N-H), 1611, 1563, 1493, 1327, 1249, 1201, 790, 700 cm^{-1}; HRMS (ESI-TOF) $[M+H]^+$ m/z calcd for $C_{19}H_{14}ClN_4O$: 349.0856; found: 349.0866. Anal. Calcd for $C_{19}H_{13}ClN_4O$: C, 65.43; H, 3.76; N, 16.06. Found C, 65.40; H, 3.83; N, 16.13.

8-(2-Amino-4-bromo-1-phenyloxy)-3-phenylbenzo[e][1,2,4]triazine (2d). Eluent: pet. ether/AcOEt, 10:2; 460 mg (52% yield) yellow crystals: mp 245 °C (MeCN); ^{1}H NMR (600 MHz, DMSO-d_6) δ 5.49 (s, 2H), 6.74 (dd, J_1 = 8.4 Hz, J_2 = 2.4 Hz, 1H), 6.97–7.01 (m, 2H), 7.07 (d, J = 2.4 Hz, 1H), 7.66 – 7.69 (m, 3H), 7.79 (dd, J_1 = 8.5 Hz, J_2 = 0.7 Hz, 1H), 8.00 (t, J = 8.2 Hz, 1H), 8.61–8.76 (m, 2H); ^{13}C NMR (151 MHz, DMSO-d_6) δ 113.1, 117.9, 118.3, 118.5, 121.7, 123.1, 128.3, 129.2, 131.8, 135.1, 137.2, 139.6, 139.7, 141.3, 142.5, 153.8, 158.9; IR (KBr) v 3290 and 3191 (N-H), 1611, 1560, 1490, 1326, 1249, 1200, 1173, 862, 790, 699 cm^{-1}; HRMS (ESI-TOF) $[M+H]^+$ m/z calcd for $C_{19}H_{14}BrN_4O$: 393.0351; found: 393.0353. Anal. Calcd for $C_{19}H_{13}BrN_4O$: C, 58.03; H, 3.33; N, 14.25. Found C, 57.97; H, 3.56; N, 14.28.

8-(2-Amino-4-trifluoromethyl-1-phenyloxy)-3-phenylbenzo[e][1,2,4] triazine (2f). Eluent: pet. ether/AcOEt, 10:2; 370 mg (48% yield) yellow crystals: mp 205-206 °C (MeCN); ^{1}H NMR (600 MHz, DMSO-d_6) δ 5.70 (s, 2H), 6.89 (dd, J_1 = 8.3 Hz, J_2 = 1.8 Hz, 1H), 7.15 (m, 2H), 7.22 (d, J = 2.1 Hz, 1H), 7.66–7.72 (m, 3H), 7.88 (d, J = 8.3 Hz, 1H), 8.05 (t, J = 8.2 Hz, 1H), 8.66 – 8.72 (m, 2H); ^{13}C NMR (151 MHz, DMSO-d_6) δ 112.0 (J = 3.2 HZ), 112.6 (J = 4.2 Hz), 114.7, 120.8, 122.7, 124.9 (q, J = 272.0 Hz), 126.8 (q, J = 31.3 Hz), 128.3, 129.3, 131.8, 135.0, 137.2, 139.7, 141.1, 141.5, 143.9, 153.0, 159.0; IR (KBr) v 3301 and 3194 (N-H), 1563, 1500, 1441, 1327, 1250, 1203, 1133, 886, 789, 701 cm^{-1}; HRMS (ESI-TOF) $[M+H]^+$ m/z calcd for $C_{20}H_{14}F_3N_4O$: 383.1120; found:

383.1133. Anal. Calcd for $C_{20}H_{13}F_3N_4O$: C, 62.83; H, 3.43; N, 14.65. Found C, 62.73; H, 3.55; N, 14.79.

8-(2-Amino-4-methoxy-1-phenyloxy)-3-phenylbenzo[e][1,2,4]triazine (2g). Eluent: pet. ether/AcOEt, 10:2. 420 mg (55 % yield) yellow crystals: mp 227 °C (MeCN); ^{1}H NMR (600 MHz, DMSO-d_6) δ 3.74 (s, 3H), 5.14 (s, 2H), 6.25 (dd, J_1 = 8.7 Hz, J_2 = 3.0 Hz, 1H), 6.49 (d, J = 3.0 Hz, 1H), 6.90 (dd, J_1 = 7.9 Hz, J_2 = 1.0 Hz, 1H), 7.02 (d, J = 8.7 Hz, 3H), 7.66–7.69 (m, 3H), 7.74 (dd, J_1 = 8.5 Hz, J_2 = 1.0 Hz, 1H), 7.98 (t, J = 8.2 Hz, 1H), 8.66–8.69 (m, 2H); ^{13}C NMR (151 MHz, DMSO-d_6) δ 55.0, 101.1, 101.8, 111.9, 120.7, 122.3, 128.3, 129.2, 131.7, 133.9, 135.2, 137.3, 139.5, 141.2, 141.6, 155.0, 157.7, 158.8; IR (KBr) v 3306 and 3193 (N-H), 1631, 1564, 1508, 1438, 1383, 1327, 1252, 1209, 852, 792, 701 cm^{-1}; ESI-HRMS (ESI-TOF) $[M+H]^+$ m/z calcd for $C_{20}H_{17}N_4O_2$: 345.1352; found: 345.1353. Anal. Calcd for $C_{20}H_{16}N_4O_2$: C, 69.76; H, 4.68; N, 16.27. Found C, 69.60; H, 4.65; N, 16.41.

2. NMR spectra

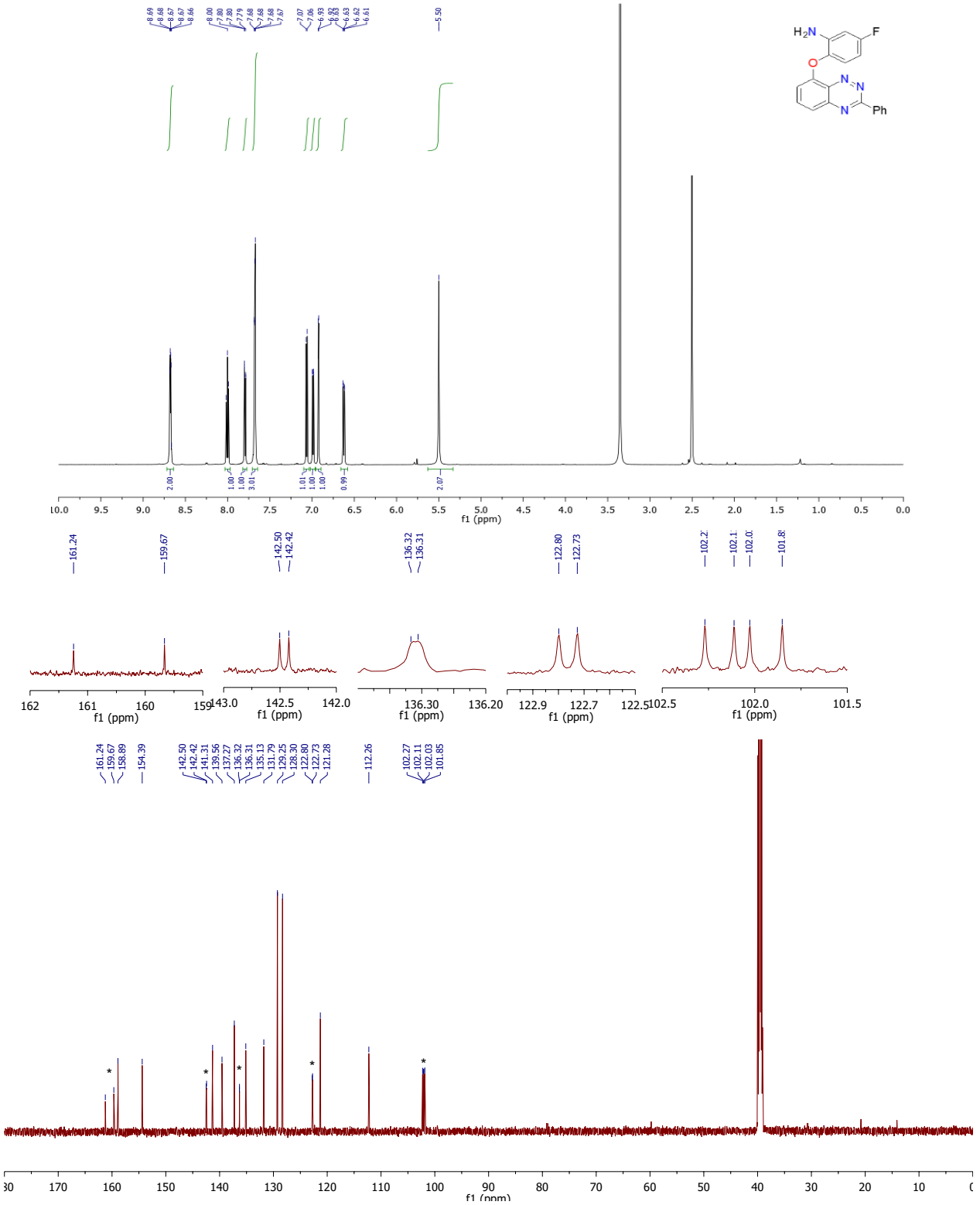

Figure S1. ^{1}H NMR (DMSO-d_6, 600 MHz) and ^{13}C NMR (DMSO-d_6, 151 MHz) spectra of **2b**. The asterisks denote signals split by ^{19}F, which are expanded above.

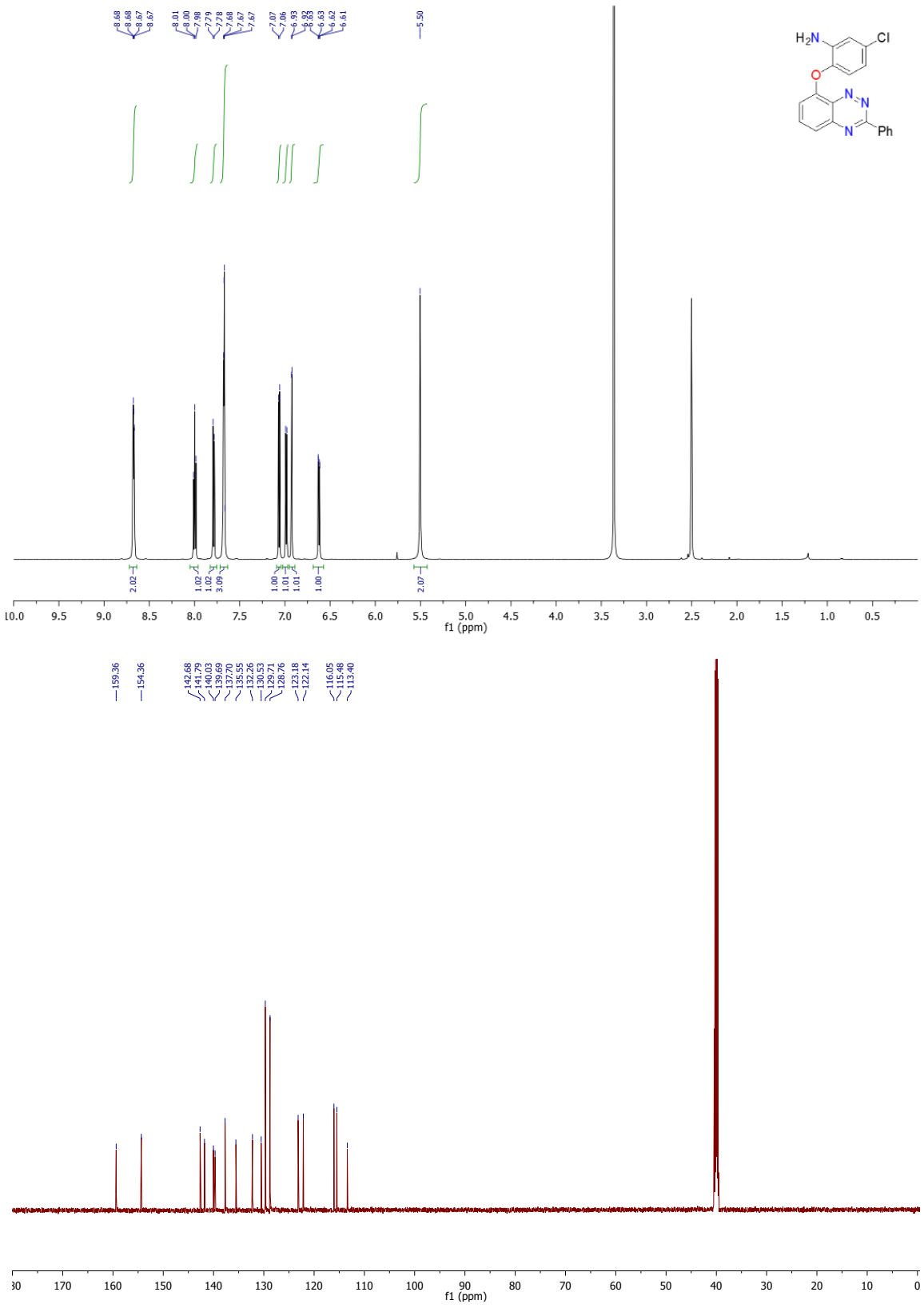

Figure S2. ^{1}H NMR (DMSO-d_6, 600 MHz) and ^{13}C NMR (DMSO-d_6, 151 MHz) spectra of **2c**.

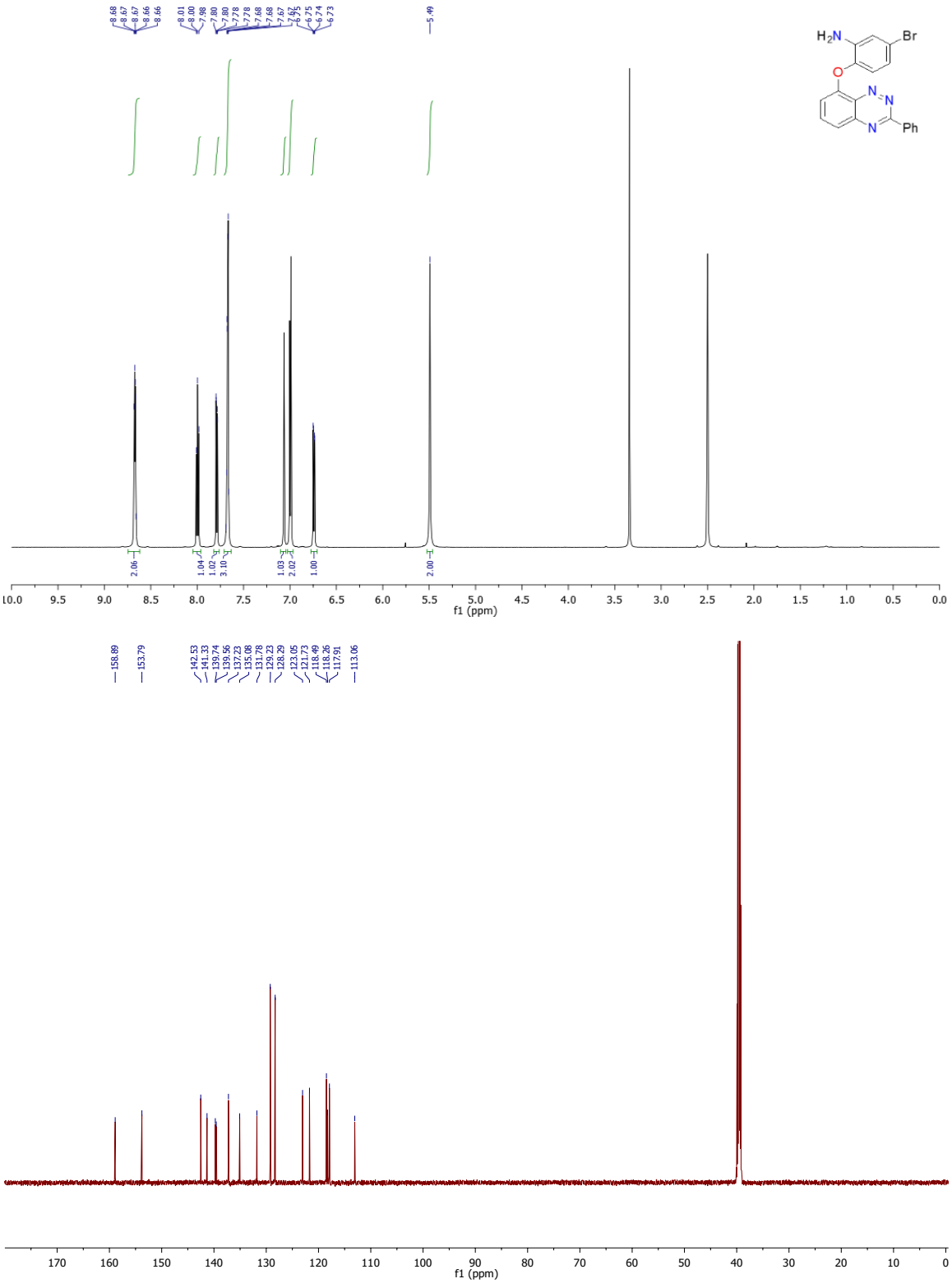

Figure S3. ^{1}H NMR (DMSO-d_6, 600 MHz) and ^{13}C NMR (DMSO-d_6, 151 MHz) spectra of **2d**.

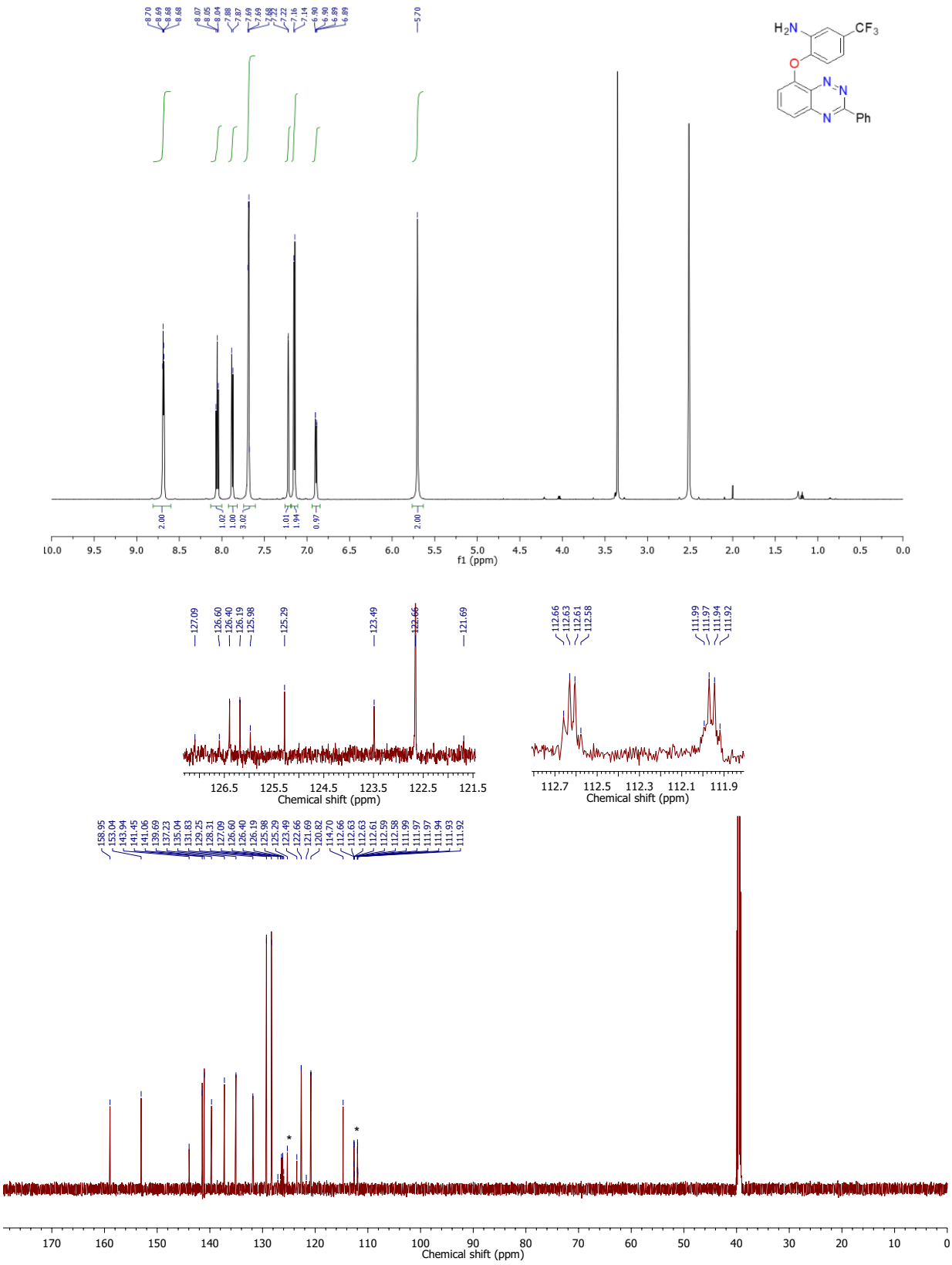

Figure S4. ^{1}H NMR (DMSO-d_6, 600 MHz) and ^{13}C NMR (DMSO-d_6, 151 MHz) spectra of **2f**.

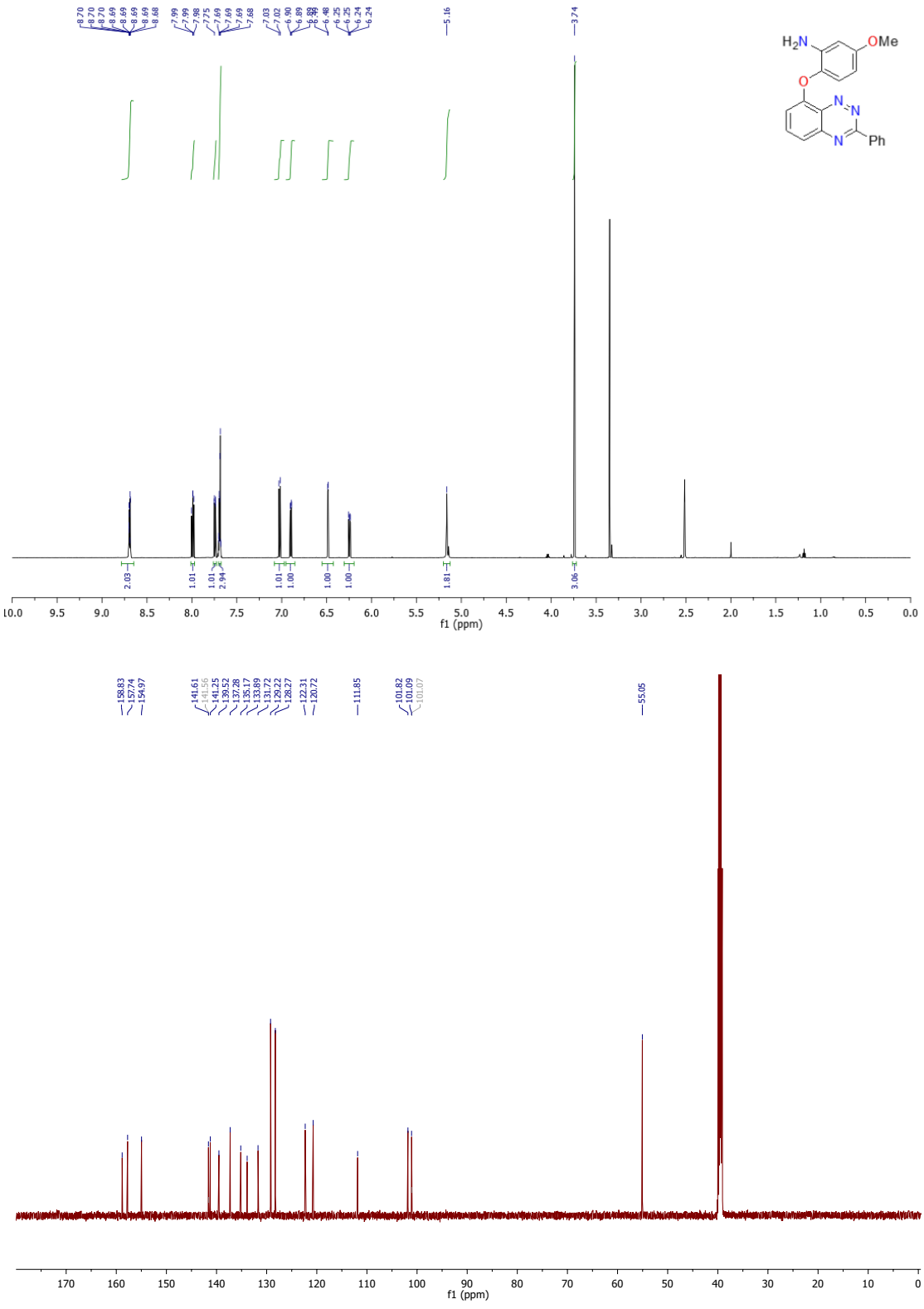

Figure S5. ^{1}H NMR (DMSO-d_6, 600 MHz) and ^{13}C NMR (DMSO-d_6, 151 MHz) spectra of **2g**.

3. XRD data collection, refinement and information

Data collection. A suitable crystal of **1f** was selected and measured on a XtaLAB Synergy, Dualflex, Pilatus 300K diffractometer. The crystal was kept at 100.0(1) K during data collection. The measurement was conducted using the CuK_α radiation (λ=1.54184 Å. The data was integrated using CrysAlisPro program.[3] Absorption intensities were corrected using SCALE3 ABSPACK scaling algorithm implemented in CrysAlisPro program.[3] Additional crystal and refinement information are listed in Table S2.

CCDC: 1988466 contains the supplementary crystallographic data for this paper. The data is provided free of charge by The Cambridge Crystallographic Data Centre via www.ccdc.cam.ac.uk/structures.

Table S2. Selected Structural Data for **1f**.

	1f [CCDC: 1988466]
Formula	$C_{20}H_{11}F_3N_3O$
Formula Weight	366.32
Crystal System	Monoclinic
Space Group	$P2_1/n$
a/Å	7.5809(2)
b/Å	19.0996(2)
c/Å	11.1263(3)
α/°	90
β/°	104.022(2)
γ/°	90
Volume/Å^3	1563.00(6)
Z	4
2θ range for data collection/°	9.26 to 158.22
Index ranges	-9 ≤ h ≤ 9, -24 ≤ k ≤ 24, -13 ≤ l ≤ 14
No. of measured, independent, and observed [$I>2\sigma(I)$] reflections	32254, 3349, 3158
*R*int	0.0276
Goodness-of-fit on F^2	1.066
Final *R* indexes [$F^2>2\sigma(F^2)$]	R_1=0.0352, w*R*2= 0.1020
Final *R* indexes [all data]	R_1=0.0367, w*R*2= 0.1036
Data/restraints/parameters	3349/0/244
Largest diff. peak/hole Å^{-3}	0.29/-0.35

Structure solution and refinement

The structure was solved with the ShelXT[4] structure solution program using Intrinsic Phasing and refined in the ShelXle by the full-matrix least-squares minimization on F^2 with the ShelXL[5] refinement package. The space group $P2_1/n$ with Z = 4 was determined based on systematic absences and intensity statistics. All non-hydrogen atoms were refined anisotropically and C–H hydrogens were generated geometrically using the HFIX command as in ShelXL. Hydrogen atoms were refined isotropically and constrained to ride on their parent atoms. The final full matrix least squares refinement converged to R_1 = 0.0352 and wR_2 = 0.1020 ($F^2 > 2\sigma(F^2)$). The crystal data and structure refinement descriptors are presented in Table S1. The molecular structure and partial packing diagrams are shown in Figures S6 – S8.

Structure Information

The structure of 10-trifluoromethyl derivative **1f** was determined with the single crystal XRD analysis. Results show that **1f** crystallizes in the monoclinic space group P21/n. The asymmetric unit contains one molecule adopting a nearly planar conformation (Figure S6), with dimensions of the heterocyclic skeleton consistent with those found in the parent radical **1a**.[2] Molecules of **1f** are arranged in nearly evenly spaced slipped stacks with the alternating interplanar distances of 3.25 and 3.07 Å. The stabilizing π···π stacking interactions are defined by significant close contacts: C(7a)···C(3a) (3.263 Å) and C(7a)···C(Ph) (3.290 Å). Neighboring stacks are connected mainly through the C-H···F interactions characterized by the donor-acceptor distance of 3.326(1) Å and the donor-hydrogen-acceptor angle of 149°.

Close contacts within the stacks of **1f**:

C(7a)···C(3a) 3.263 Å (-0.137 Å inside VDW separation)

C(7a)···C(Ph) 3.290 Å (-0.110 Å inside VDW separation)

Close contacts between the stacks of **1f**:

F···HC(8) 2.496 Å (-0.174 Å inside VDW separation)

C(Ph)···HC(8) 2.873 Å (-0.027 Å inside VDW separation)

The intramolecular inter-ring angle was calculated as the angle between two planes: one was defined by all 17 C and N atoms of the heterocyclic core and the second by six C atom of the Ph substituent. The mean plane of the heterocyclic core (defined by 17 C, N and O atoms) was used to measure the intermolecular separation within the stack and also to measure the angle between the two neighboring stacks.

Slippage angle - of 35.2° was calculated as an angle defined by O(7)···O(7)···N(12) minus 90°. The two oxygen atoms used for the measurements were for two molecules in the stack with same orientation.

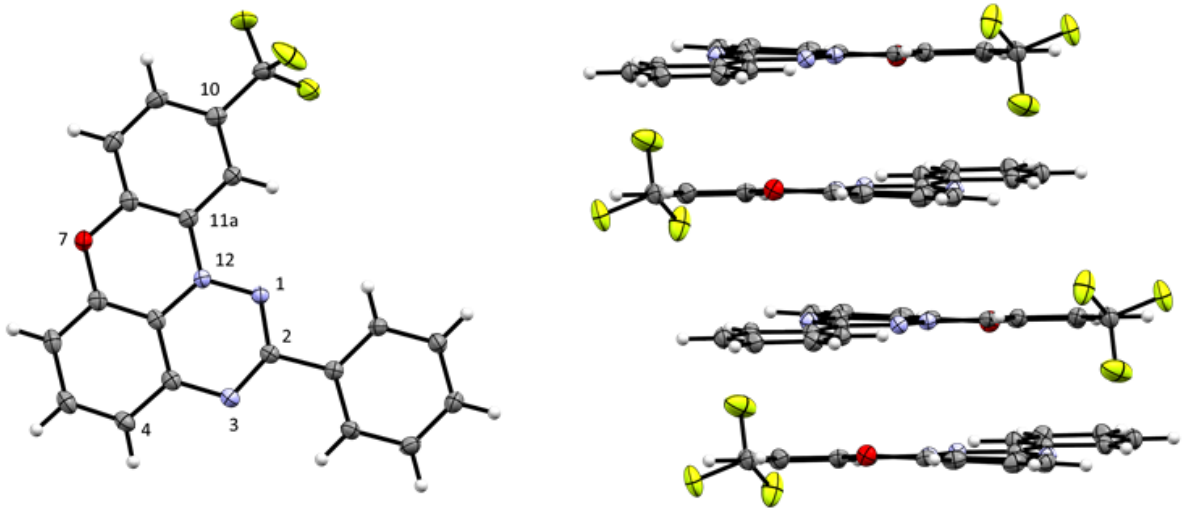

Figure S6. A displacement ellipsoid diagram for **1f** (ellipsoids set at 50% probability level). Labels according to the chemical structure.

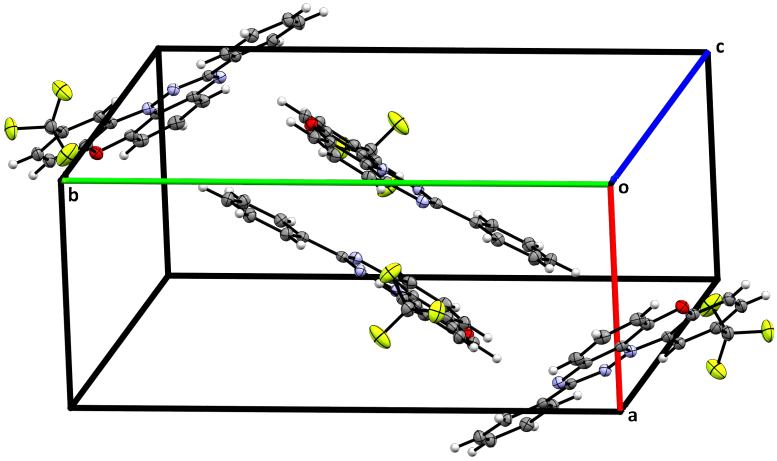

Figure S7. Packing diagram for the unit cell of **1f**.

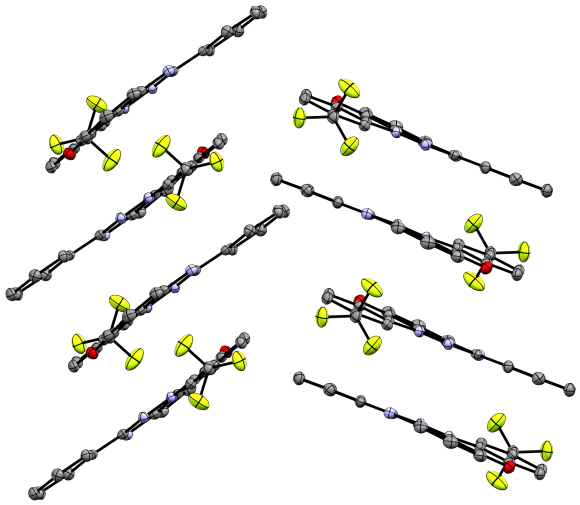

Figure S8. Partial packing diagram for **1f** showing two slipped stacks. Angle between the stacks 118.5°.

4. Electronic absorption spectroscopy

Electronic absorption spectra for radicals **A** and series **1** were recorded in spectroscopic grade CH_2Cl_2 at concentrations in a range 1–6 × 10^{-5} M and fitted to the Beer–Lambert law. Results are shown in Figures S9–S16 and summarized in Table S3.

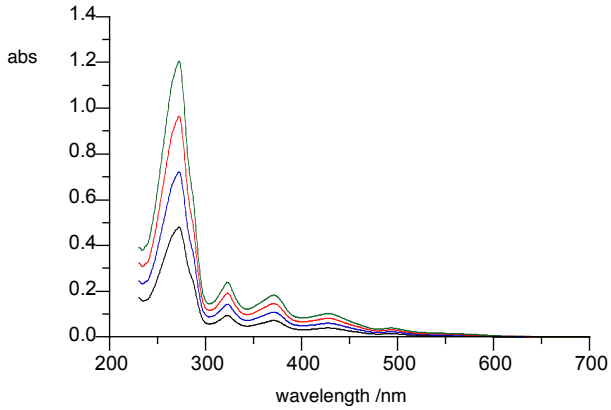

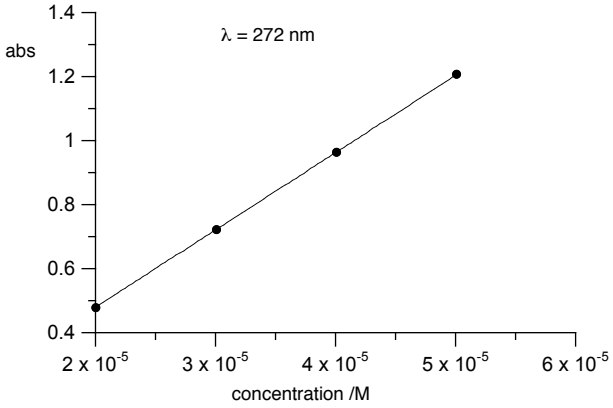

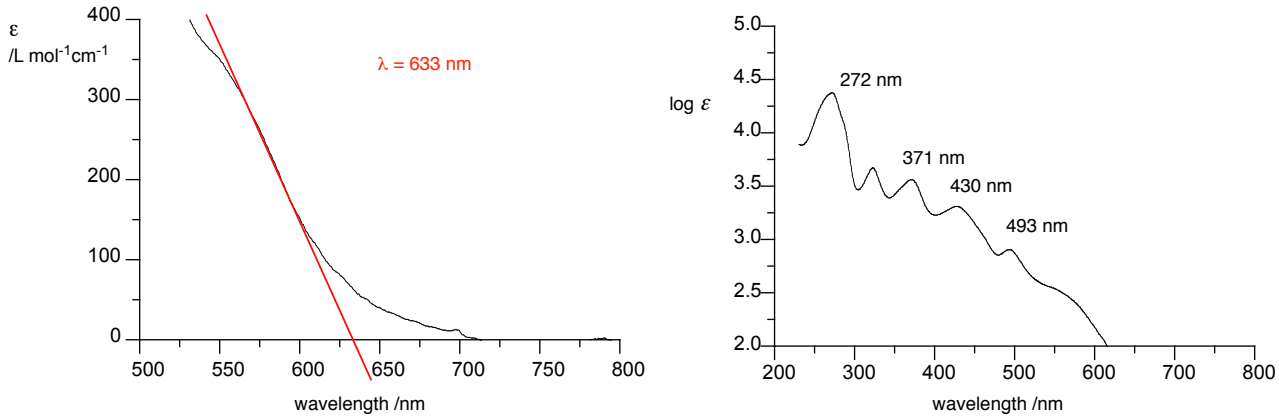

Figure S9. Clockwise: electronic absorption spectra for **A** in CH_2Cl_2 at four concentrations, determination of molar extinction coefficient ε at λ = 272 nm (best fit function: ε = 24145×conc, r^2 = 0.9999), molar extinction *log* (ε) plot, and onset of absorption (optical band-gap).

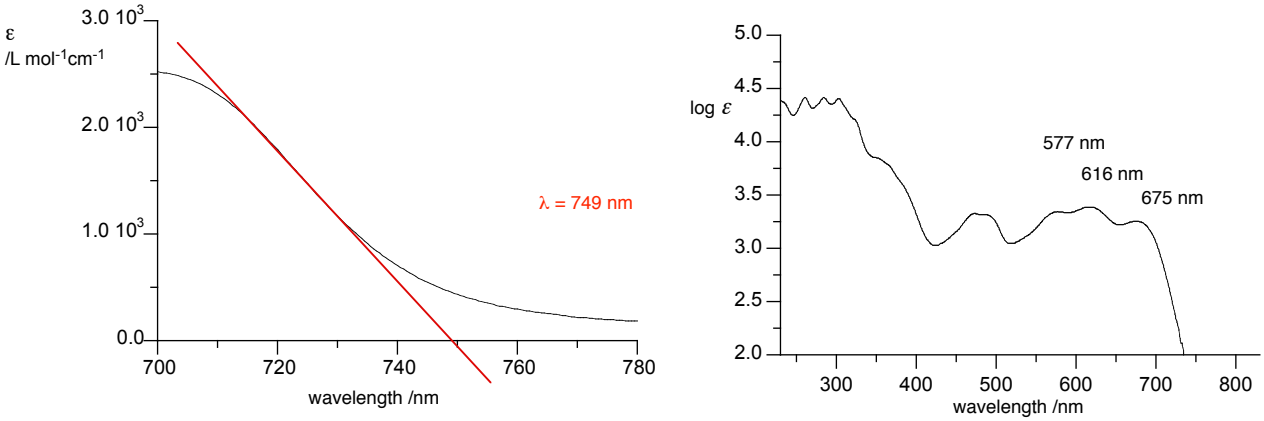

Figure S10. Electronic absorption spectra for **1a** in CH_2Cl_2. Left: onset of absorption (optical band-gap). Right: molar extinction *log* (ε) plot.[2]

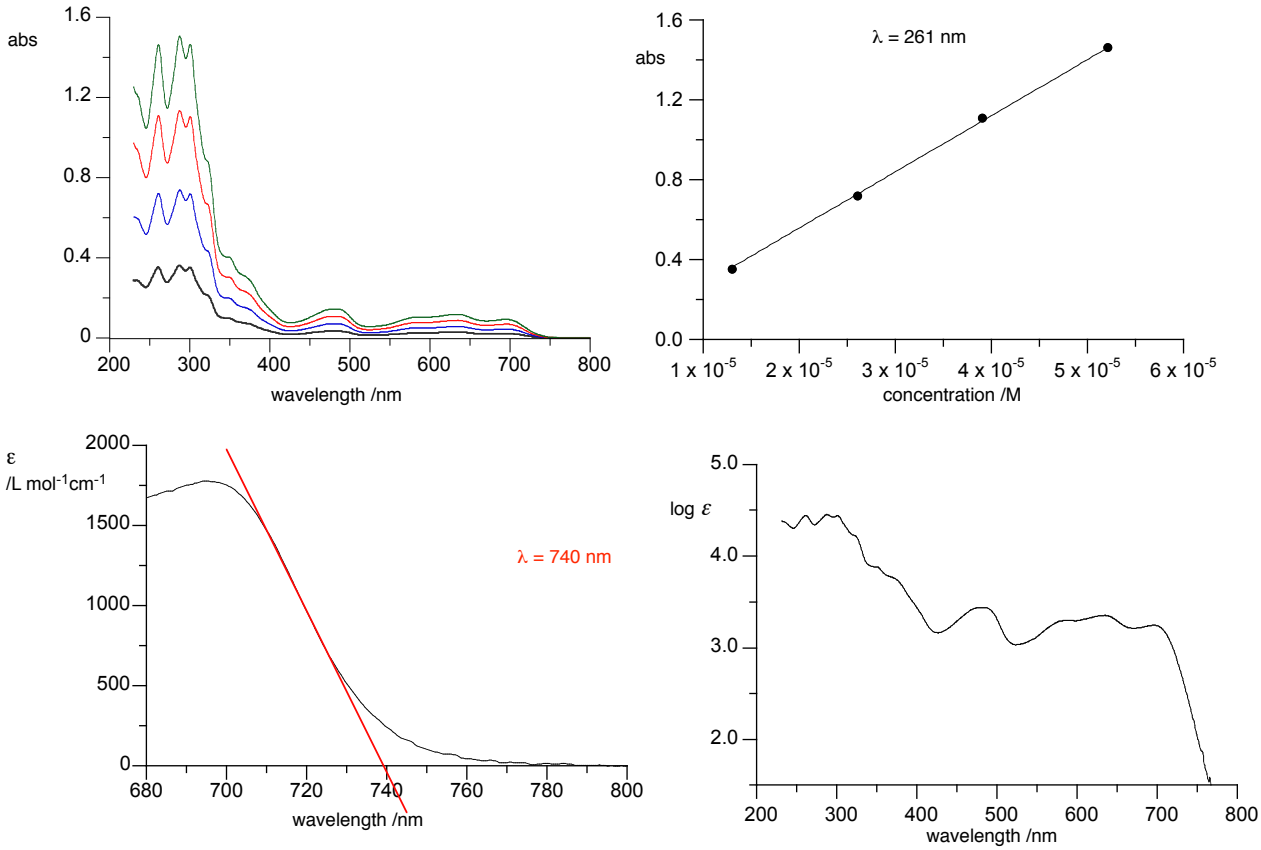

Figure S11. Clockwise: electronic absorption spectra for **1b** (X=F) in CH_2Cl_2 for four concentrations, determination of molar extinction coefficient ε at λ = 261 nm (best fit function: ε = 28057×conc, r^2 = 0.9994), molar extinction *log* (ε) plot, and onset of absorption (optical band-gap).

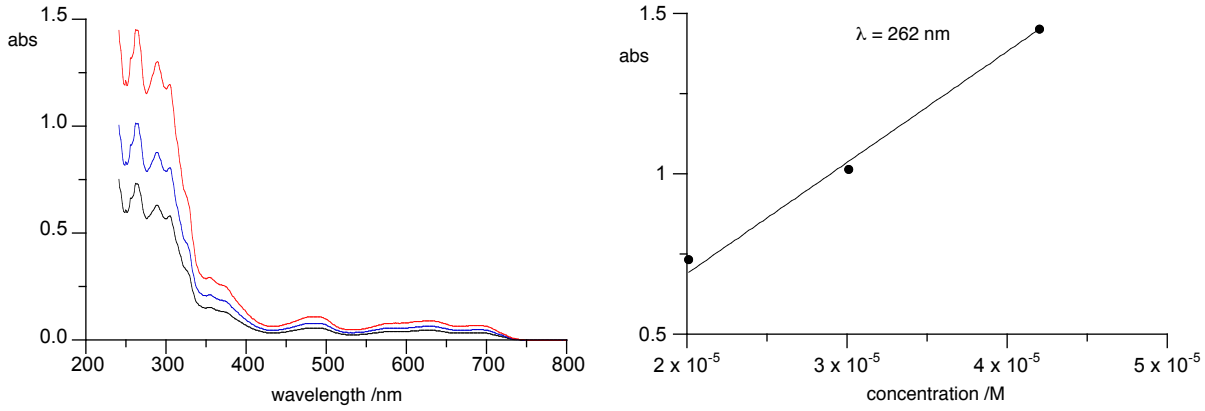

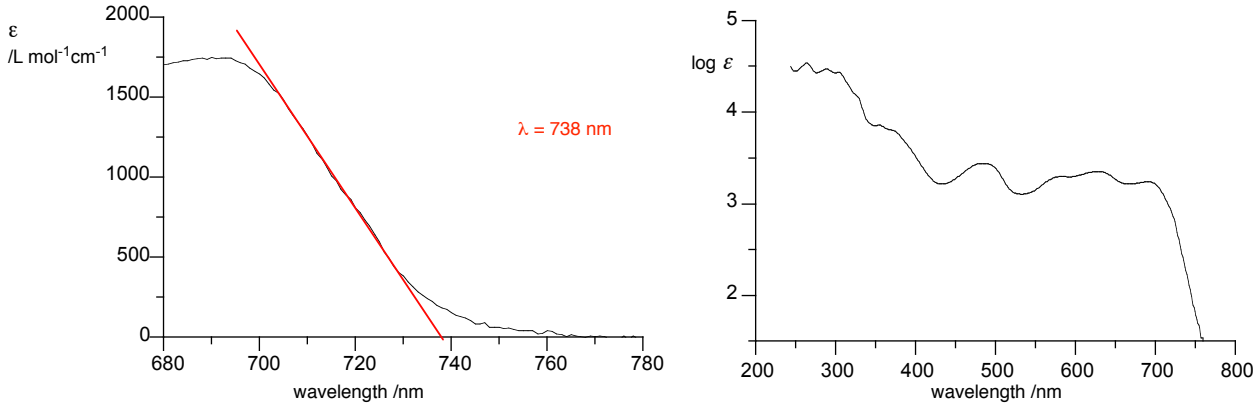

Figure S12. Clockwise: electronic absorption spectra for **1c** (X=Cl) in CH_2Cl_2 for three concentrations, determination of molar extinction coefficient ε at λ = 262 nm (best fit function: ε = 34563×conc, r^2 = 0.992), molar extinction *log* (ε) plot, and onset of absorption (optical band-gap).

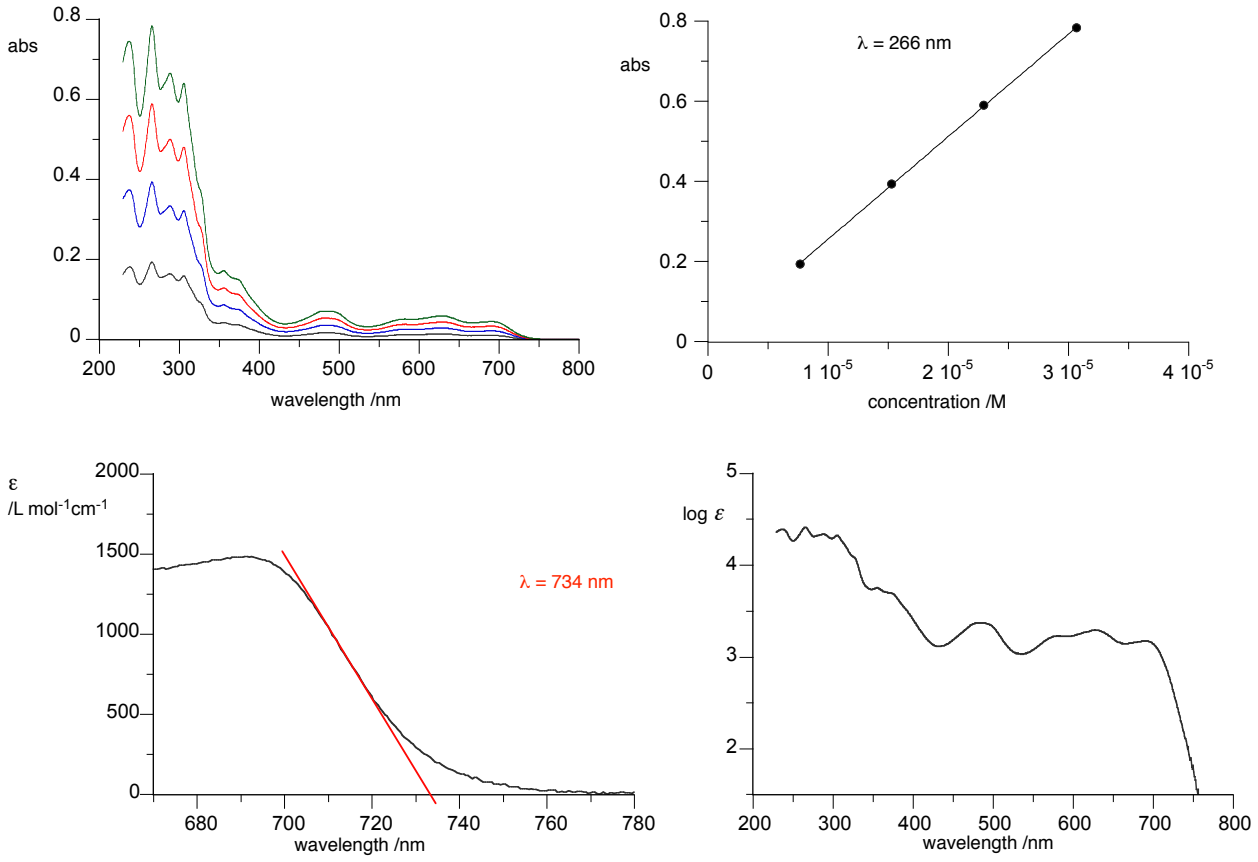

Figure S13. Clockwise: electronic absorption spectra for **1d** (X=Br) in CH_2Cl_2 for four concentrations, determination of molar extinction coefficient ε at λ = 266 nm (best fit function: ε = 25582×conc, r^2 = 0.9999), molar extinction *log* (ε) plot, and onset of absorption (optical band-gap).

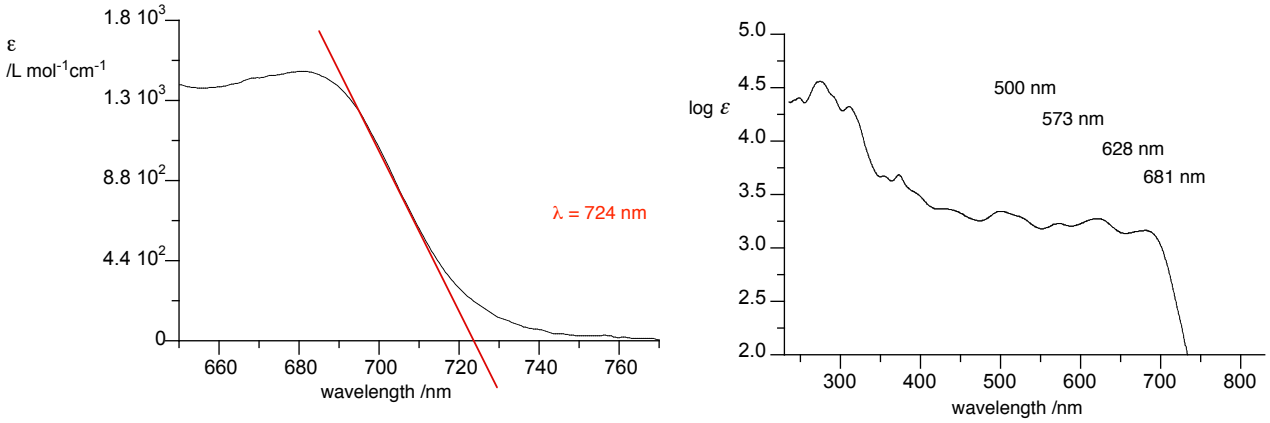

Figure S14. Electronic absorption spectra for **1e** (X=CN) in CH_2Cl_2. Left: onset of absorption (optical band-gap). Right: molar extinction *log* (ε) plot.[1]

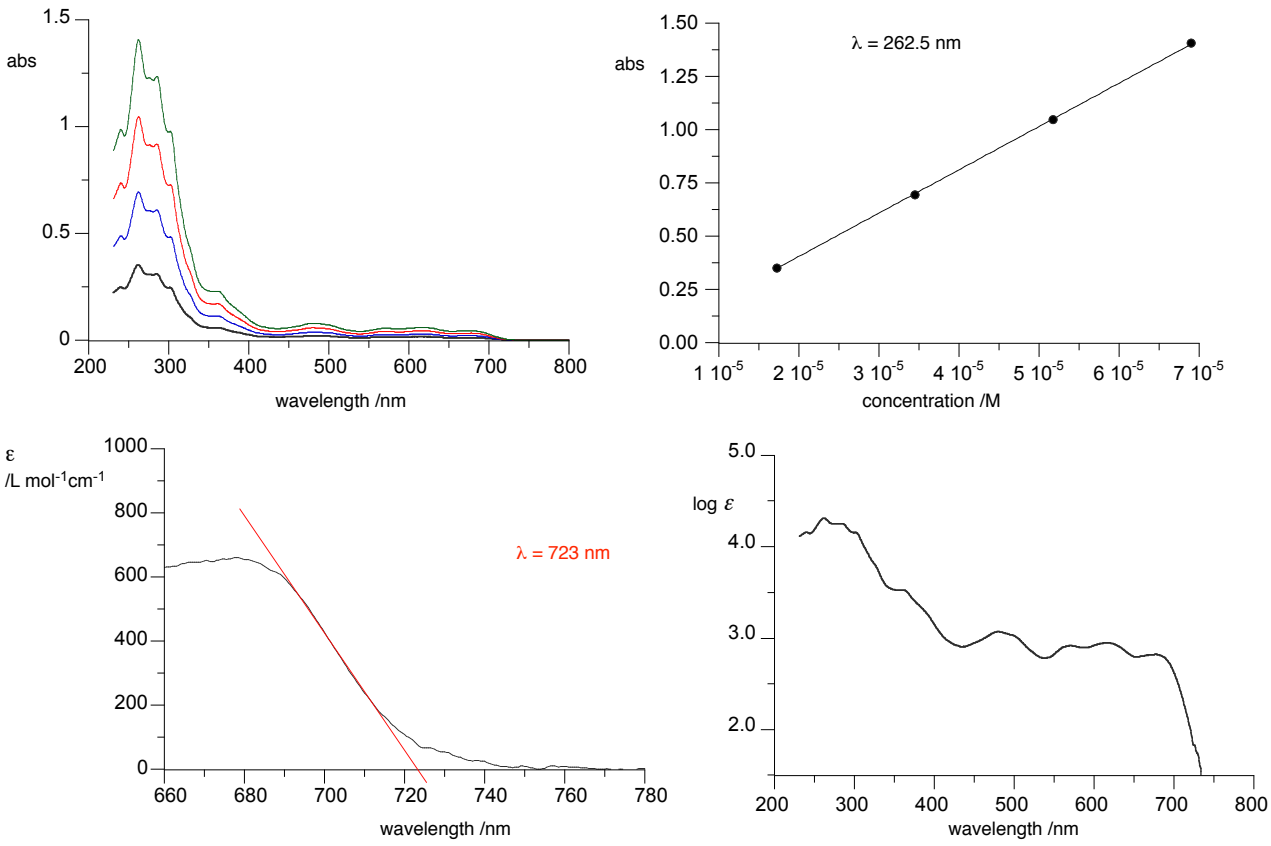

Figure S15. Clockwise: electronic absorption spectra for **1f** (X=CF_3) in CH_2Cl_2 for four concentrations, determination of molar extinction coefficient ε at λ = 262.5 nm (best fit function: ε = 20290×conc, r^2 = 0.9999), molar extinction *log* (ε) plot, and onset of absorption (optical band-gap).

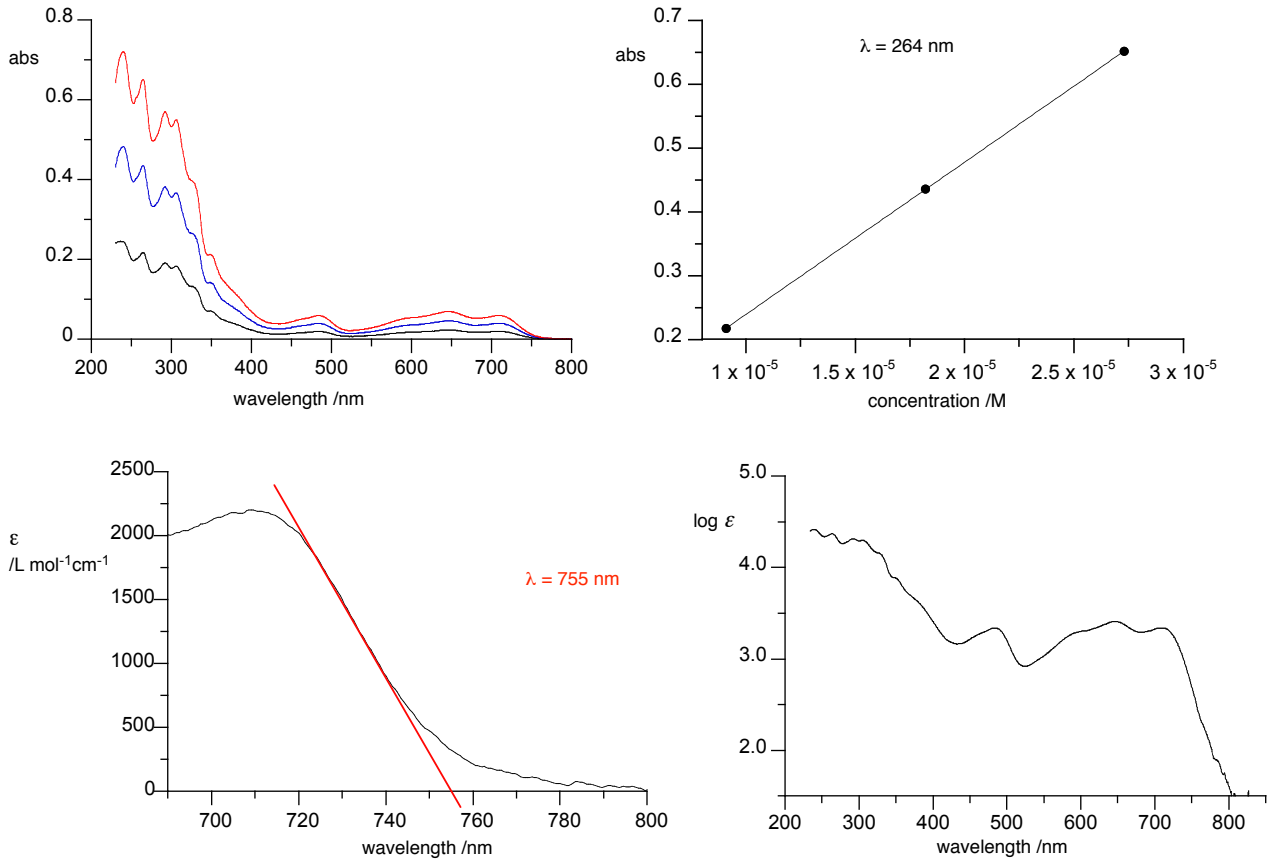

Figure S16. Clockwise: electronic absorption spectra for **1g** (X=OCH_3) in CH_2Cl_2 for three concentrations, determination of molar extinction coefficient ε at λ = 264 nm (best fit function: ε = 23889×conc, r^2 = 0.9999), molar extinction *log* (ε) plot, and onset of absorption (optical band-gap).

Table S3. Summary of the absorption maxima and *log*(ε) for radicals **A** and **1**.

Radical	λ_{max} /nm		
	range I (<400 nm)	range II (400-550 nm)	range III (>550 nm)
A	272 (4.38), 323 (3.68), 3.71 (3.57)	430 (3.31) 493 (2.91)	550 sh (2.55)
1a [a] X = H	261 (4.42), 284 (4.42), 303 (4.41), 350sh (3.85)	473 (3.33) 488 (3.32)	577 (3.35), 616 (3.39), 675 (3.26)
1b X = F	261 (4.45), 288 (4.46), 301 (4.44), 322sh (4.23), 350 (3.89)	484 (3.44)	586 (3.30), 634 (3.36), 695 (3.25)
1c X = Cl	262 (4.53), 289 (4.47), 304 (4.44), 374sh (3.79)	482 (3.44)	583 (3.30), 629 (3.36), 692 (3.24)
1d X = Br	266(4.41), 288(4.34), 306 (4.32), 355 (3.75), 370sh (3.70)	482 (3.37)	582 (3.23), 628 (3.29), 691 (3.17)
1e [b] X = CN	248 (4.41), 274 (4.56), 311 (4.33), 354 (3.68), 373 (3.69)	428 (3.37) 500 (3.35)	573 (3.23), 621 (3.28), 681 (3.17)
1f X = CF_3	262.5 (4.31), 285 (4.25), 302 (4.15), 361 (3.52)	481 (3.07), 498sh (3.03	571 (2.91), 617 (2.94), 678 (2.82)
1g X = OMe	239 (4.42), 264 (4.38), 292 (4.32), 305 (4.30, 324sh (4.17), 347sh (3.89)	483 (3.34)	602sh (3.30), 646 (3.41), 709 (3.34)

[a] Ref. [2]. [b] Ref. [1].

5. Ultraviolet photoelectron spectra.

The UV-PES spectra were recorded on a home-built (IPREM), three-part spectrometer equipped with a main body device, He-I radiation source (21.21 eV and/or 48 eV) and a 127° cylindrical analyzer. The spectrometer works at constant analyzer energy under 5×10^{-6} hPa working pressure and $\leq 10^{-7}$ hPa for channeltron (X914L) pressure. The monitoring is done by a microcomputer supplemented by a digital–analogue converter (AEI spectrum). The spectra resulting from a single scan are built from 2048 points and are accurate within 0.05 eV. Spectra are calibrated with lines of xenon (12.13 and 13.44 eV) and of argon (15.76 and 15.94 eV). The accuracy of the ionization energies is ±0.03 eV for sharp peaks and ± 0.05 eV for broad and overlapping signals. The samples were slowly vaporized under low pressure (1.3×10^{-6} hPa) inside a handmade three-valve injector

(3/4 inch diameter; 10 cm length; working temperature: –190 °C ≤ T ≤ +300 °C), and the gaseous flow was then continuously and simultaneously analyzed by UV-photoelectron spectrometer.

Evaporation and (melting point) temperatures are as follows: **A**, 115 ºC (110 ºC); **1a**, 175 ºC (176 ºC); **1b**, 163 ºC (180 ºC); **1c**, 202 ºC (201 ºC); **1d**, 201 ºC (210 ºC); **1e**, 202 ºC (202 ºC); **1f**, 180 ºC (164 ºC); **1g**, 180 ºC (165 ºC).

Results are graphically shown in Figure 4 in the main text and are summarized in Table S4.

For comparison purposes onset of the HOMO was determined for **A** and **1** as is shown in Figure S17 and listed in Table S4.

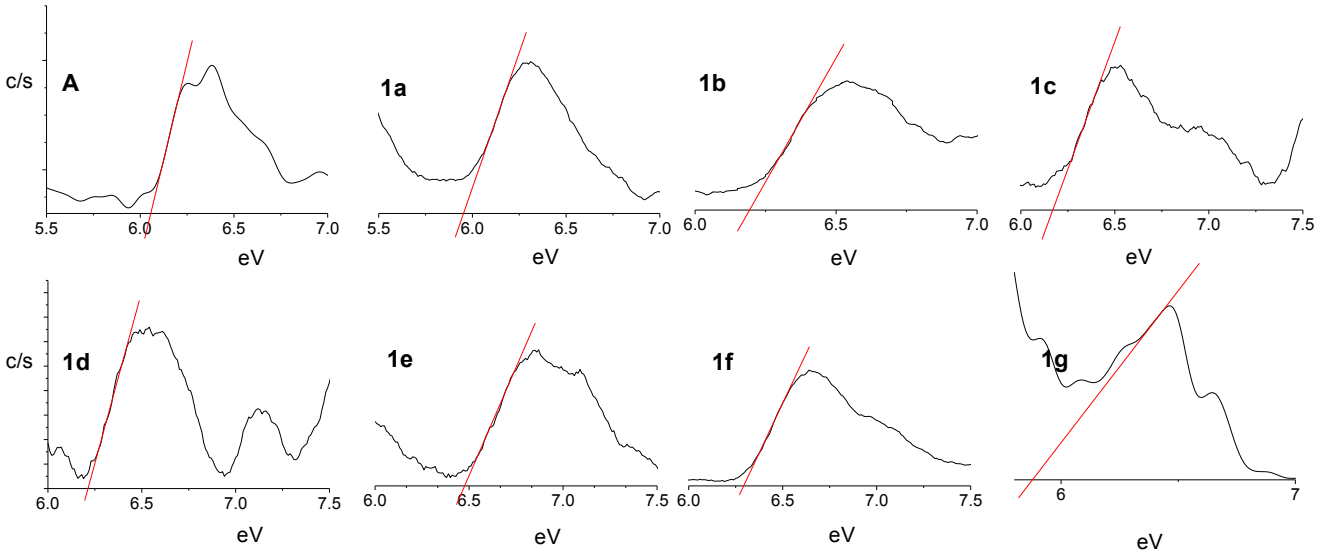

Figure S17. Determination of the onset of the HOMO in UV-photoelectron spectra for Blatter radical **A** and derivatives **1**.

Table S4. Summary of for UV-PES spectra for radicals **A** and **1**.

Compound	IE_n /eV	Onset of IE_1 /eV
A	6.40, 7.98, 8.82, 9.31	6.05
1a, X = H	6.45, 7.74, 8.74, 9.03	5.95
1b, X = F	6.55, 7.84, 8.69, 9.32	6.19
1c, X = Cl	6.50, 7.71, 8.75, 9.03	6.17
1d, X = Br	6.51, 7.70, 8.76, 9.06	6.21
1e, X = CN	6.80, 8.22, 8.93, 9.56	6.48
1f, X = CF_3	6.56, 8.05, 8.72, 9.50	6.29
1g, X = OMe	6.45, 7.67, 8.54, 9.29	5.88

6. Electrochemical data

The electrochemical characterization of selected radicals was conducted using BioLogic SP-200 potentiostat/galvanostat instrument in dry and degassed CH_2Cl_2 (concentration 0.5 mM) in the presence of $[n\text{-}Bu_4N]^+[PF_6]^-$ as an electrolyte (concentration 50 mM) using glassy carbon as the working electrode and Ag/AgCl as the reference electrode with a scan rate of 50 mV s^{-1} at *ca.* 20 ^oC. In the end of each measurement decamethylferrocene was added and the peak potentials were referenced to the $FcMe_{10}/FcMe_{10}^+$ couple. The oxidation potential for the $FcMe_{10}/FcMe_{10}^+$ couple was established at –0.10 V *vs* SCE by comparison with the oxidation potential for the Fc/Fc^+ couple (0.46 V *vs* SCE).[6]

Cyclic voltammetry (CV) plots are shown in Figures S18–S23 and numerical result are shown in Table 4 in the main text.

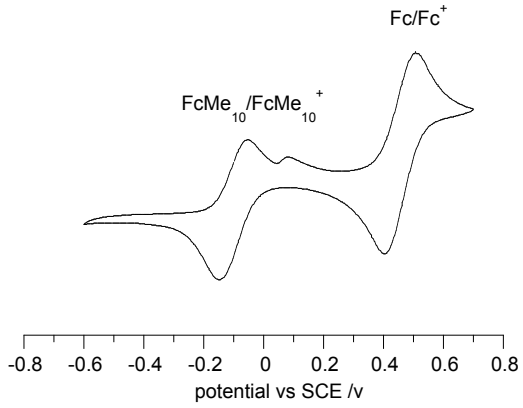

Figure S18. Cyclic voltammogram for ferrocene (Fc) and decamethylferrocene ($FcMe_{10}$). The small peak at about 0.05 V is related to some impurity in the commercial $FcMe_{10}$.

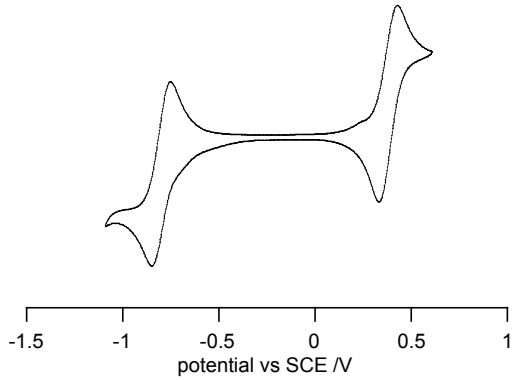

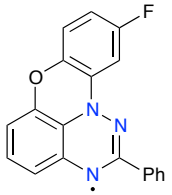

Figure S19. Cyclic voltammogram for **1b**.

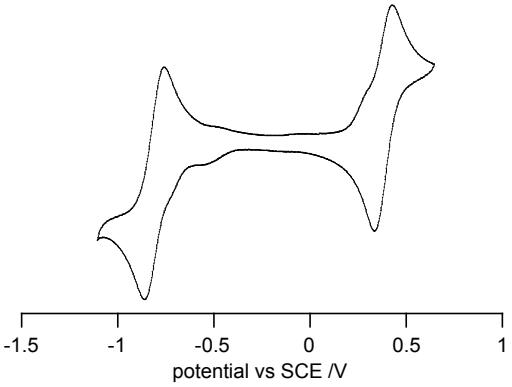

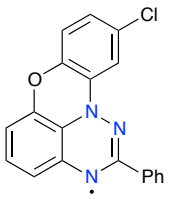

Figure S20. Cyclic voltammogram for **1c**.

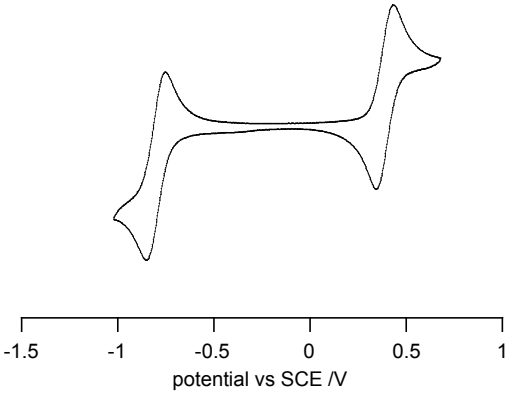

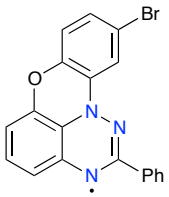

Figure S21. Cyclic voltammogram for **1d**.

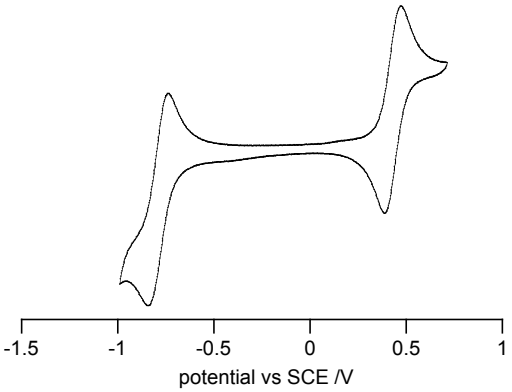

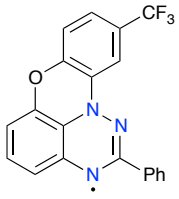

Figure S22. Cyclic voltammogram for **1f**.

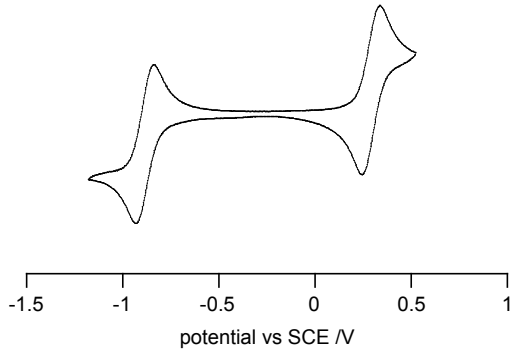

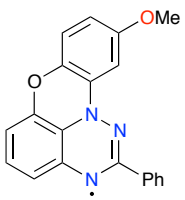

Figure S23. Cyclic voltammogram for **1g**.

For comparison with solid-state organic semiconductors, a comparison of onset of anodic oxidation peak and onset of the HOMO (from the UV-PES) are shown in Table S5.

Table S5. A comparison of onset values for oxidation potential $E_{1/2}^{0/+1}$ and ionization energy IE_1.

radical	$E_{1/2}^{0/+1}$ onset *vs* Fc/Fc^+ /V	IE_1 onset /eV
A	-0.27	6.05
1a	-0.21	5.95
1b	-0.17	6.19
1c	-0.20	6.17
1d	-0.14	6.21
1e	-0.35	6.48
1f	-0.11	6.29
1g	-0.25	5.88

7. EPR spectroscopy

EPR spectra for radicals **1** were recorded on an X-band EMX-Nano EPR spectrometer at ambient temperature on dilute and degassed solutions in distilled benzene in a concentration range of $1–2\times10^{-4}$ M. The microwave power was set with the Power Sweep program below the saturation of the signal, modulation frequency of 100 kHz, modulation amplitude of 0.5 G_{pp} and spectral width of 100 G. Accurate *g*-values were obtained using TEMPO as EMX-Nano internal standard.

Simulations of the spectra were performed with EasySpin (Matlab) using all EPR-active nuclei and results of DFT calculations as the starting point for simulations. The chemically equivalent nuclei (H in the Ph substituent and F in the CF_3 group) were treated as a group of 2 or 3 identical nuclei, respectively. The resulting *hfcc* values were perturbed several times until a global minimum for the fit was achieved. For consistency, EPR spectra for **A**, **1a** and **1e** were recorded again and simulated with EasySpin. Experimental and simulated spectra are shown in Figures S24–S28 and numerical values are collected in Table S6.

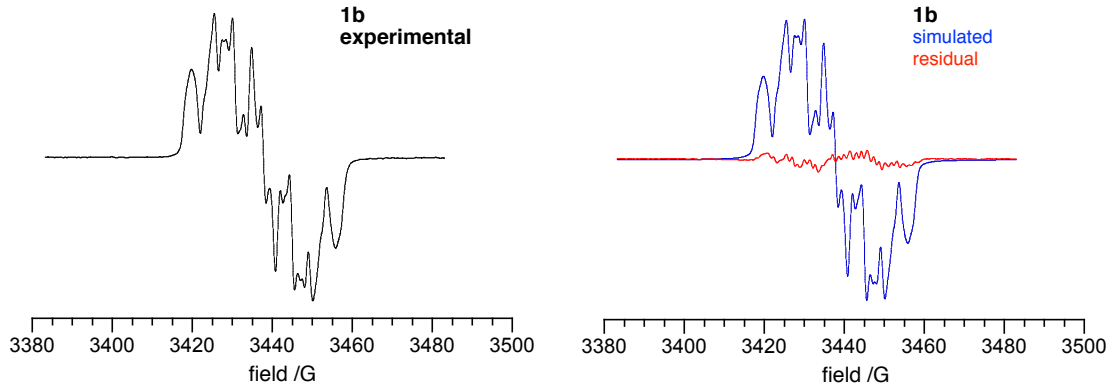

Figure S24. Experimental (black, left), simulated (blue, right) and difference (red, right) spectra for **1b** recorded in benzene at *ca* 20 °C.

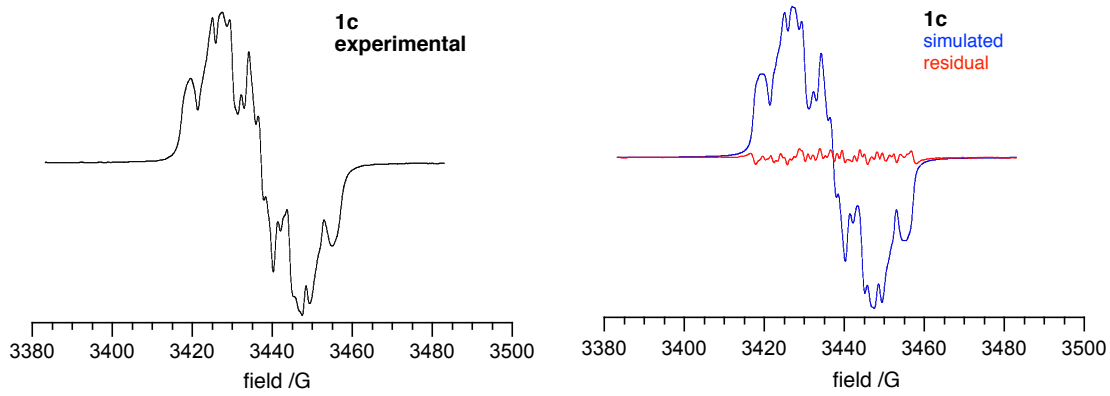

Figure S25. Experimental (black, left), simulated (blue, right) and difference (red, right) spectra for **1c** recorded in benzene at *ca* 20 °C.

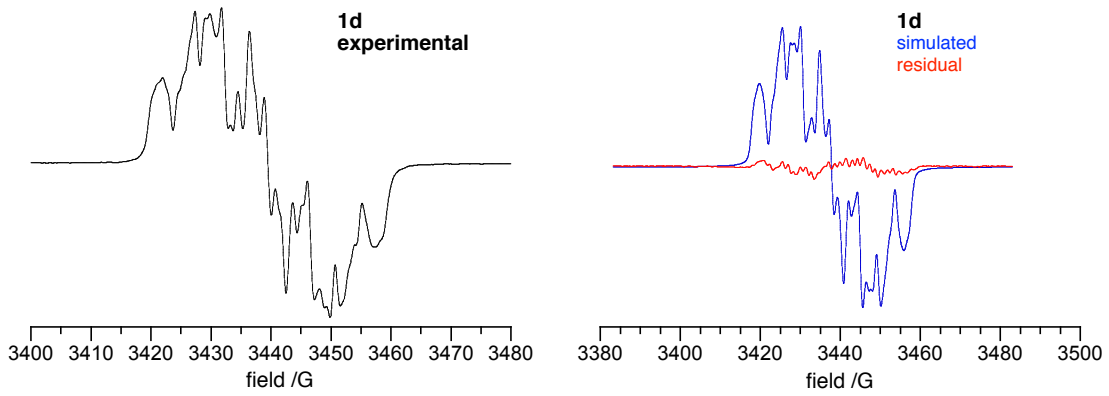

Figure S26. Experimental (black, left), simulated (blue, right) and difference (red, right) spectra for **1d** recorded in benzene at *ca* 20 °C.

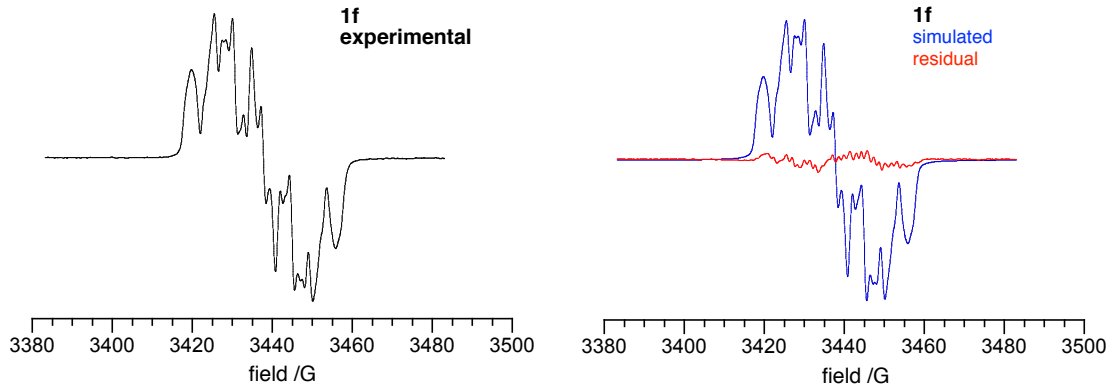

Figure S27. Experimental (black, left), simulated (blue, right) and difference (red, right) spectra for **1f** recorded in benzene at *ca* 20 °C.

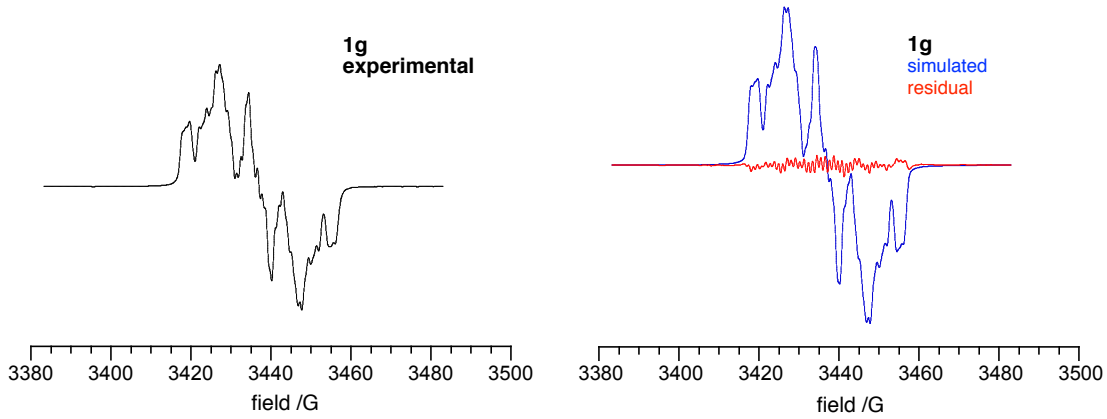

Figure S28. Experimental (black, left), simulated (blue, right) and difference (red, right) spectra for **1g** recorded in benzene at *ca* 20 °C.

Table S6. Experimental hyperfine coupling constants (G) and *g* values for radicals in series **1** recorded in benzene at *ca* 20 °C.[a]

Atom	**A**	**1a**	**1b** [b]	**1c**	**1d**	**1e**	**1f** [b]	**1g**
X =	–	H	F	Cl	Br	CN	CF_3	OMe
a_{N12}	7.56	7.51	7.15	7.15	7.15	7.03	7.11	7.37
a_{N1}	4.92	4.28	4.40	4.46	4.42	4.50	4.50	4.29
a_{N3}	4.94	4.42	4.44	4.54	4.48	4.70	4.53	4.37
						0.17(a_N)		
a_H	1.34	1.94	2.02	2.08	1.98	1.81	2.04	2.14
a_H	0.83	1.11	1.76	1.76	1.76	1.51	1.58	1.57
a_H	0.68	0.72	1.39	1.49	1.01	1.49	1.04	1.12
a_H	0.59	0.60	0.75	1.44	0.89	1.44	0.82	0.71
a_H	0.37	0.39	0.57	0.71	0.31	0.67	0.44	0.71
a_H	0.25	0.29	0.44	0.45	0.18	0.57	0.41	0.37
a_H	2x0.25	0.11	0.13	0.29	0.17	0.39	0.23	0.33
a_H	2x0.17	0.10	0.10	–	–	–	0.07	–
a_{2H}	0.11	0.09	0.08	0.05	0.28	0.10	0.05	0.23
a_{2H}	0.08	0.03	0.03	0.01	0.08	0.07	0.00	0.09
g	2.0036	2.0036	2.0038	2.0035	2.0035	2.0035	2.0039	2.0035

[a] a_N assignment based on the DFT results. See section 7e below. [b] The assignment of a_F is uncertain.

8. Correlation analysis of literature experimental data.

A selection of formal oxidation potentials $E_{1/2}^{0/+1}$ *vs* Fc/Fc^+ for selected polycyclic hydrocarbons,[7] their gas phase ionization energies[8] and solid support ionization energies[9] are collected in Table S7. A graphical correlation of the data is shown in Figure S29.

More extensive lists of experimental gas phase ionization energies for aromatic polycyclic hydrocarbons are in ref.[8, 10] and an extensive compilations of their solid-state ionization energies are in ref.[9] and oxidation potentials in ref.[11].

Table S7. Comparison of ionization energies and oxidation potentials for selected hydrocarbons.

hydrocarbon	*Gas phase* *IE* [a] /eV	*Solid sup* *IE* [b] /eV	*MeCN* $E_{1/2}^{0/+1}$ *vs* Fc/Fc$^+$ [c] /V
antracene	7.41	5.69	0.96
Benz[a]antracene	7.41	5.64	1.06
Chrysene	7.59	5.80	1.15[d]
Naphthalene	8.15	6.40	1.46
Pentacene	6.61	4.83	0.44
Perylene	6.97	5.20	0.68
Phenanthrene	7.86	6.08	1.35
Pyrene	7.41	5.58	0.98
Teteracene	6.97	5.23	0.66
Coronene	7.29	5.52	0.952 [d]

[a] Ref.[8, 10b]. [b] From Ref. [9]. [c] Measured in MeCN. The original data referenced to SCE was corrected by 0.38 V. Ref [7]. [d] Ref. [11]

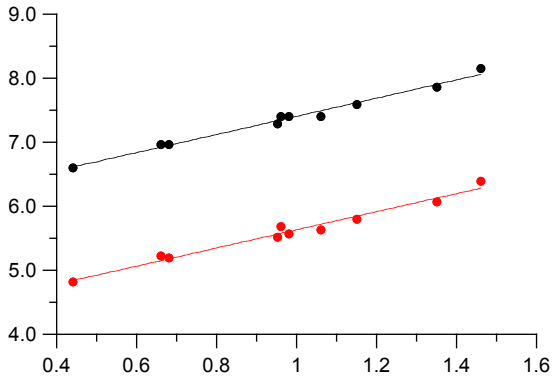

Figure S29. Correlation of experimental *IE* gas phase (black) and on solid support (red) and oxidation potentials $E^{0/+1}$ for 10 polycyclic aromatic hydrocarbons (see Table S5). Best fit function: IE_{gas} = 5.99(6)+1.42(6)× $E^{0/+1}$, r^2 = 0.985 and IE_{solid} = 4.23(8)+1.41(8)× $E^{0/+1}$, r^2 = 0.975.

Estimate of experimental electron affinities (*EA*) for radicals **A** and **1** was accomplished using correlations for literature data. Thus, a correlation function for calculation of vertical electron affinity EA_{vert} on a solid support was obtained using data reported in ref.[12] and involving

experimental EA_{vert}, acquired with the IPES method on thin films, and reduction potentials $E^{-1/0}$ relative to Fc/Fc^{+} couple for 23 structurally diverse compounds. For details and specific references see [12] The graphical correlation is shown in Figure S30.

The correlation function for calculation of adiabatic electron affinity, EA_{adiab}, was obtained using data reported in ref [13], and involving experimental EA_{adiab}, acquired with the ECD method in gas phase, and half wave reduction potentials $E_{1/2}^{-1/0}$ recorded in DMF relative to SCE for 25 structurally diverse compounds collected in ref.[13]. For details and specific references see[13]. The graphical correlation is shown in Figure S31.

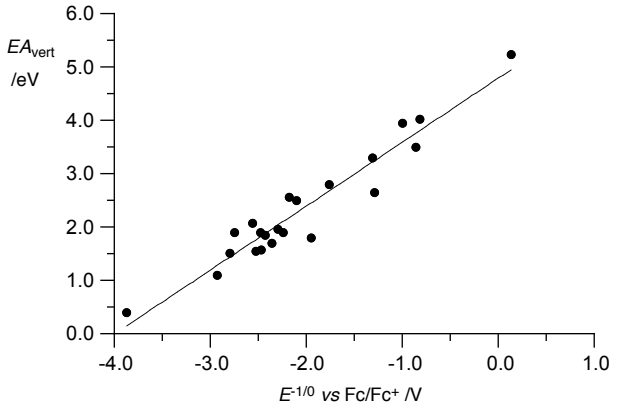

Figure S30. Correlation of experimental EA_{vert} (IPES) and reduction potentials $E^{-1/0}$ for 23 structurally diverse compounds. For details and specific references see [12]. Best fit function: $EA_{vert} = 4.79(17)+1.20(8)\times E^{-1/0}$, $r^2 = 0.923$.

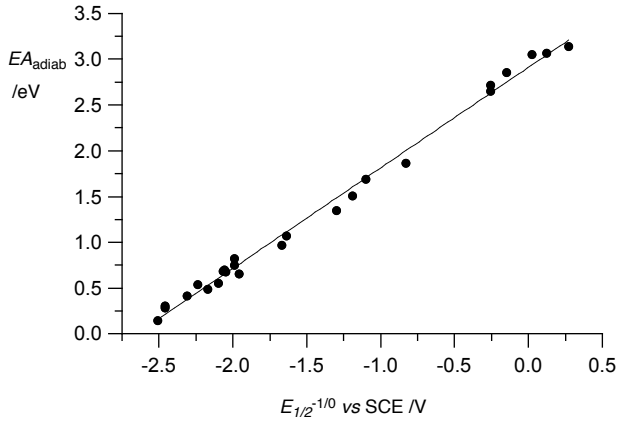

Figure S31. Correlation of experimental EA_{adiab} (ECD) and reduction potentials $E_{1/2}^{-1/0}$ in DMF for 25 structurally diverse compounds. For details and specific references see [13]. Best fit function: $EA_{adiab} = 2.92(3)+1.10(2)\times E_{1/2}^{-1/0}$, $r^2 = 0.994$.

Correlation of the optical band gap and the difference of vertical ionization energy IE_{vert} and vertical electron affinity EA_{vert} (transport gap energy) using data set (except for benzene) from ref [12] is shown in Figure S32. Since the error on the intercept was nearly twice larger than the value itself, it was fixed at 0. The resulting slope value of 1.25 is smaller that that derived in another work (1.37).[14]

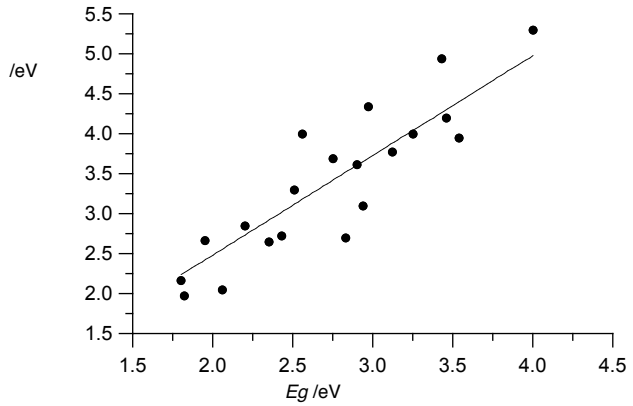

Figure S32. Correlation of experimental difference $IE_{vert} - EA_{vert}$ and optical band gap. For details and specific references see [12]. Best fit function: $IE_{vert} - EA_{vert} = 1.25(3) \times E_g$, $r^2 = 0.79$.

9. Computational details and results

a) General. All fully unrestricted open shells calculations were performed using the Gaussian 09[15] computational package. All geometry optimizations were carried out with the range-separated hybrid CAM-B3LYP[16] functional and the triple-ζ 6-311G(d,p)[17] basis set, including Cl and Br, without symmetry constraints. Results are shown in Table S8. Frequency calculations were performed for the optimized geometries in order to verify that the stationary points obtained were true energy minima. Additional Rydberg functions (6-311++G(d,p)) are included in the basis set to improve the description of the electron affinities (*EA*) and UV-vis calculations. Avogadro software[18] was used as a tool for visualization of molecular orbitals.

b) Molecular geometry. Molecular geometry of radicals **1a**–**1g** was optimized at the UCAM-B3LYP/6-311G(d,p) level of theory and compared with experimental data for **1a**[2] and **1f**. The relative deviation (Δ%) from the experimental data is within the range of [-2.4;2.9]% for **1a** and [-0.9;0.9]% for **1f**. Analysis of DFT-derived geometrical parameters in series **1** shows that the

substituent X noticeably impacts distances between the oxygen atom and its two vicinal carbon atoms, C(6a)–O(7) and O(7)–C(7a). Thus, as the electron withdrawing character of X increases the asymmetry of the bond length changes from $d_{6a\text{-}7} < d_{7\text{-}7a}$, in derivatives **1a**, **1b**, and **1g**, through $d_{6a\text{-}7} \approx d_{7\text{-}7a}$, in **1c** and **1d**, to $d_{6a\text{-}7} > d_{7\text{-}7a}$ in **1e** and **1f**.

Table S8. UCAM-B3LYP/6-311G(d,p) molecular geometry parameters for radicals **1** and experimental X-ray diffraction data for **1a** and **1f** (bond angles in Å, angles in degrees).

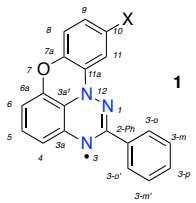

Bond length and angle	**1a**, X = H			**1b**	**1c**	**1d**	**1e**	**1f**, CF_3			**1g**
		XRD [a]	Δ%	F	Cl	Br	CN		XRD	Δ%	OMe
10-X	1.082	—	—	1.343	1.746	1.900	1.431	1.498	—	—	1.355
11a-12	1.404	1.42	1.1	1.400	1.401	1.402	1.401	1.402	1.401	-0.1	1.402
12-1	1.343	1.35	0.5	1.343	1.343	1.343	1.343	1.343	1.354	0.8	1.344
1-2	1.336	1.32	-1.2	1.336	1.337	1.337	1.337	1.337	1.343	0.4	1.336
2-2Ph	1.487	1.50	0.9	1.487	1.487	1.487	1.486	1.486	1.485	-0.1	1.488
2-3	1.325	1.364	2.9	1.325	1.325	1.325	1.325	1.325	1.337	0.9	1.324
3-3a	1.366	1.38	1.0	1.366	1.366	1.366	1.365	1.366	1.375	0.7	1.367
3a-3a^1	1.401	1.38	-1.5	1.401	1.401	1.401	1.401	1.401	1.407	0.4	1.402
3a^1-6a	1.393	1.36	-2.4	1.393	1.393	1.393	1.392	1.392	1.393	0.1	1.394
6a-7	1.368	1.39	1.6	1.368	1.370	1.370	1.373	1.372	1.381	0.7	1.365
7-7a	1.372	1.381	0.7	1.373	1.370	1.370	1.364	1.367	1.379	0.9	1.376
12-1-2	116.1	114.1	-1.8	116.0	116.1	116.1	116.1	116.1	115.1	-0.9	116.0
1-2-3	127.2	130.2	2.3	127.1	127.1	127.1	127.0	127.0	128.5	1.2	127.2
6a-7-7a	118.2	118.5	0.3	118.2	118.2	118.2	118.4	118.4	117.7	-0.6	118.0
9-10-X	120.2	—	—	119.0	119.5	119.5	120.0	119.8	—	—	116.0
11-10-X	119.5	—	—	118.5	119.0	119.1	119.7	119.4	—	—	124.0
3a^1-12-11a	118.7	118.6	-0.1	118.7	118.7	118.7	118.7	118.7	119.1	0.3	118.6

[a] Data form ref. [2]

c) Ionization Energies (*IE*$_n$). Vertical IE_n were calculated using two methods at the UCAM-B3LYP/6-311G(d,p) level of theory. In the first, frequently used method[19] the lowest ionization energy (IE_1) was calculated as $\Delta E_{SCF} = E_{SCFcation} - E_{SCFradical}$ for fully optimized radical in its ground state and the cation at the radical geometry (single point calculations). Higher vertical ionization energies (IE_n) were obtained as a sum of ΔE_{SCF} and $E_{TD\text{-}DFT(n)}$, where the latter is the E_n excitation energy calculated with the TD method for the cation at the radical geometry. The TD method takes

into account also low-lying ionic states and this approach has been demonstrated to be particularly reliable for obtaining accurate ionization energies.[20] The results are shown in Table 3 for **1b** (main text) and Tables S8–S15 for **A** and all radicals in series **1**.

In the second method, vertical ionization energies (IE_n) are calculated based on Koopmans' theorem[21] and "shifted eigenvalue" correction previously suggested by Stowasser and Hoffmann.[22] Koopmans' theorem[21] was originally developed for closed-shell systems and assumed that $IE_n = -\varepsilon_{MO}$, where ε_{MO} is the energy of the occupied molecular orbital. This formalism adopted for analysis of open-shell molecules takes the form for the first ionization energy: $IE_1^{KS} = -\varepsilon_{SOMO}^{KS}$ where ε_{SOMO}^{KS} is the Kohn-Sham energy of the highest occupied MO (SOMO) of the radical in its ground state, obtained with the unrestricted method (UCAM-B3LYP/6-311G(d,p)). Following the Stowasser and Hoffmann suggestion,[22] ionization energies for the first and higher ionization can be calculated from Kohn-Sham orbital energy corrected by a constant factor x, $IE_n = -\varepsilon_{HOMO-n+1}^{KS} + x$, where the $\varepsilon_{HOMO-n+1}^{KS}$ for n > 1 is obtained for fully geometry-optimized radical using restricted open-shell method (RO-CAM-B3LYP/6-311G(d,p)). The "shifted eigenvalue" correction x is calculated as $x_{\Delta ESCF\ or\ exp} = IE_1^{ref(\Delta ESCF\ or\ exp)} - IE_1^{KS}$ using either theoretical first ionization energy as the reference (if $IE_1^{ref(\Delta ESCF)} = \Delta E_{\mathrm{SCF}} = E_{\mathrm{SCFcation}} - E_{\mathrm{SCFradical}}$, *vide supra*, then $x_{\Delta ESCF} = IE_1^{ref(\Delta ESCF)} - IE_1^{KS}$) or experimentally determined first ionization energy as the reference (if $IE_1^{ref(exp)} = IE_1^{exp}$ then $x_{exp} = IE_1^{exp} - IE_1^{KS}$).[23] Results obtained using both methods are shown in Tables S9–S16.

A comparison of experimental and theoretical IE_1 is shown in Table S17.

Table S9. Assignment of experimental ionization energies (IE_n) for radical **A**. Theoretical values were obtained with the CAM-B3LYP/6-311G(d,p) method. See text for details.

A 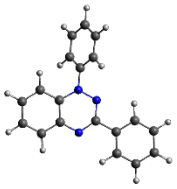 Type of MO	**Method 1** $IE_1 = \Delta E_{SCF}$ $IE_n = \Delta E_{SCF}+E_{TDDFT}$ /eV	**Method 2** $-\varepsilon^{KS}$ /eV	Corrected $-\varepsilon^{KS} + x_{\Delta SCF}$ $x_{\Delta SCF} = 0.319$ /eV	Corrected $-\varepsilon^{KS} + x_{exp}$ $x_{exp} = 0.312$ /eV	Exp. IE_n /eV
H(S)OMO 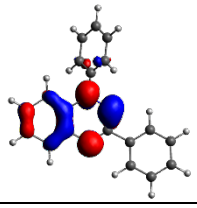	6.407	6.088	6.407	6.40	**6.40**
HOMO–1 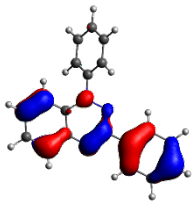	7.698	7.649	7.968	7.96	**7.98**
HOMO–2 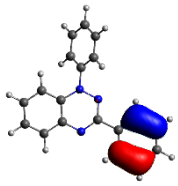	8.515	8.270	8.589	8.58	**8.82**
HOMO–3 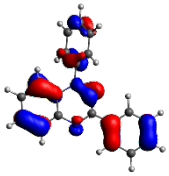	8.710	8.428	8.747	8.74	**8.82**
HOMO–4 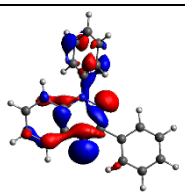	8.824	8.679	8.998	8.99	**9.31**
HOMO–5 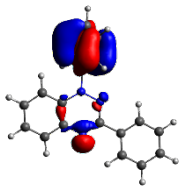	8.976	8.937	9.256	9.25	**9.31**

Table S10. Assignment of experimental ionization energies (IE_n) for radical **1a**. Theoretical values were obtained with the CAM-B3LYP/6-311G(d,p) method. See text for details.

1a, 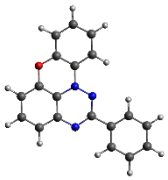 Type of MO	**Method 1** $IE_1 = \Delta E_{SCF}$ $IE_n = \Delta E_{SCF} + E_{TDDFT}$ /eV	**Method 2**			Exp. IE_n /eV
		$-\varepsilon^{KS}$ /eV	Corrected $-\varepsilon^{KS} + x_{\Delta SCF}$ $x_{\Delta SCF} = 0.320$ /eV	Corrected $-\varepsilon^{KS} + x_{exp}$ $x_{exp} = 0.337$ /eV	
H(S)OMO 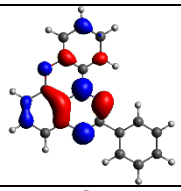	6.432	6.113	6.432	6.45	**6.45**
HOMO–1 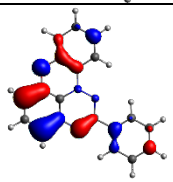	7.334	7.310	7.629	7.65	**7.74**
HOMO–2 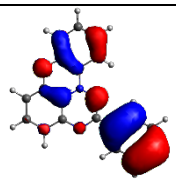	8.472	8.196	8.515	8.53	**8.74**
HOMO–3 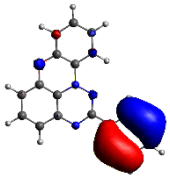	8.487	8.373	8.693	8.71	**8.74**
HOMO –4 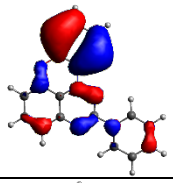	9.027	8.827	9.147	9.165	**9.03**
HOMO –5 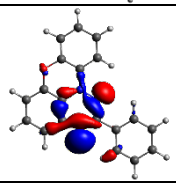	9.028	8.889	9.209	9.23	**9.03**

Table S11. Assignment of experimental ionization energies (IE_n) for radical **1b**. Theoretical values were obtained with the CAM-B3LYP/6-311G(d,p) method. See text for details.

1b, Type of MO 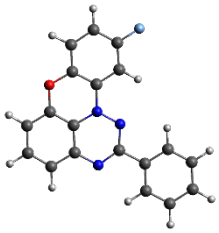	**Method 1** $IE_1 = \Delta E_{SCF}$ $IE_n = \Delta E_{SCF} + E_{TDDFT}$ /eV	**Method 2** $-\varepsilon^{KS}$ /eV	Corrected $-\varepsilon^{KS} + x_{\Delta SCF}$ $x_{\Delta SCF} = 0.322$ /eV	Corrected $-\varepsilon^{KS} + x_{exp}$ $x_{exp} = 0.291$ /eV	Exp. IE /eV
H(S)OMO 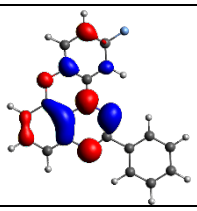	6.581	6.259	6.581	6.55	**6.55**
HOMO–1 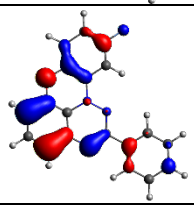	7.416	7.382	7.704	7.67	**7.84**
HOMO–2 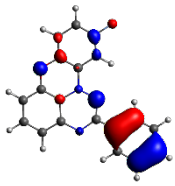	8.532	8.250	8.572	8.54	**8.69**
HOMO–3 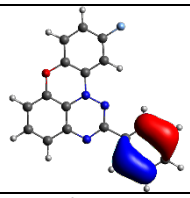	8.561	8.428	8.750	8.72	**8.69**
HOMO–4 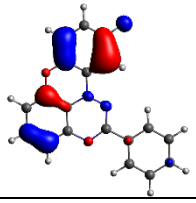	9.092	8.965	9.287	9.26	**9.32**
HOMO–5 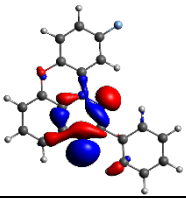	9.140	9.007	9.329	9.30	**9.32**

Table S12. Assignment of experimental ionization energies (IE_n) for radical **1c**. Theoretical values were obtained with the CAM-B3LYP/6-311G(d,p) method. See text for details.

1c 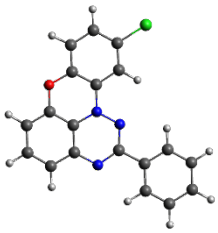 Type of MO	**Method 1** $IE_1 = \Delta E_{SCF}$ $IE_n = \Delta E_{SCF} + E_{TDDFT}$ /eV	**Method 2** $-\varepsilon^{KS}$ /eV	Corrected $-\varepsilon^{KS} + x_{\Delta SCF}$ $x_{\Delta SCF} = 0.297$ /eV	Corrected $-\varepsilon^{KS} + x_{exp}$ $x_{exp} = 0.199$ /eV	Exp. IE /eV
H(S)OMO 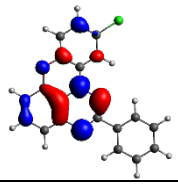	6.598	6.301	6.598	6.50	**6.50**
HOMO–1 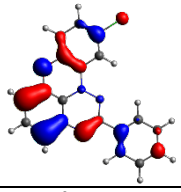	7.456	7.436	7.733	7.635	**7.71**
HOMO–2 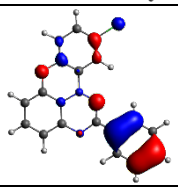	8.554	8.269	8.566	8.47	**8.75**
HOMO–3 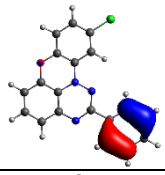	8.585	8.442	8.739	8.64	**8.75**
HOMO–4 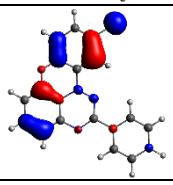	9.110	8.935	9.232	9.13	**9.03**
HOMO–5 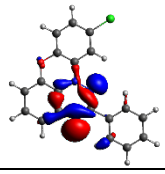	9.159	9.040	9.337	9.24	**9.03**

Table S13. Assignment of experimental ionization energies (IE_n) for radical **1d**. Theoretical values were obtained with the CAM-B3LYP/6-311G(d,p) method. See text for details.

1d 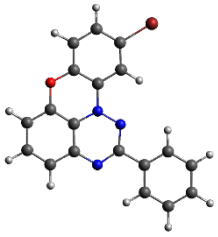 Type of MO	**Method 1** $IE_1 = \Delta E_{SCF}$ $IE_n = \Delta E_{SCF}+E_{TDDFT}$ /eV	**Method 2** $-\varepsilon^{KS}$ /eV	Corrected $-\varepsilon^{KS} + x_{\Delta SCF}$ $x_{\Delta SCF} = 0.288$ /eV	Corrected $-\varepsilon^{KS} + x_{exp}$ $x_{exp} = 0.218$ /eV	Exp. IE /eV
H(S)OMO 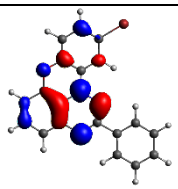	6.580	6.292	6.580	6.51	**6.51**
HOMO–1 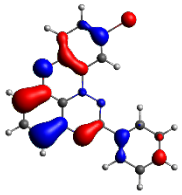	7.439	7.423	7.711	7.64	**7.70**
HOMO–2 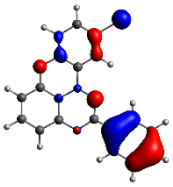	8.540	8.246	8.533	8.46	**8.76**
HOMO–3 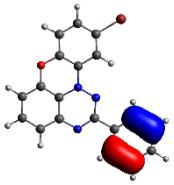	8.566	8.436	8.724	8.65	**8.76**
HOMO–4 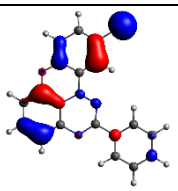	9.093	8.826	9.114	9.04	**9.06**
HOMO–5 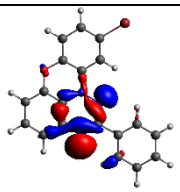	9.145	9.031	9.319	9.25	**9.06**

Table S14. Assignment of experimental ionization energies (IE_n) for radical **1e**. Theoretical values were obtained with the CAM-B3LYP/6-311G(d,p) method. See text for details.

1e 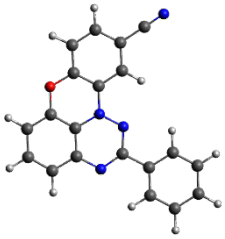 Type of MO	**Method 1** $IE_1 = \Delta E_{SCF}$ $IE_n = \Delta E_{SCF}+E_{TDDFT}$ /eV	**Method 2** $-\varepsilon^{KS}$ /eV	Corrected $-\varepsilon^{KS} + x_{\Delta SCF}$ $x_{\Delta SCF} = 0.291$ /eV	Corrected $-\varepsilon^{KS} + x_{exp}$ $x_{exp} = 0.309$ /eV	Exp. IE /eV
H(S)OMO 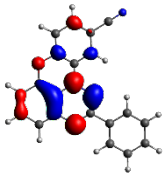	6.782	6.491	6.782	6.80	**6.80**
HOMO–1 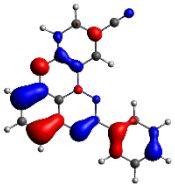	7.688	7.657	7.948	7.97	**8.22**
HOMO–2 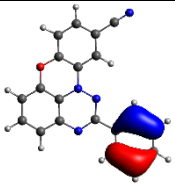	8.701	8.430	8.720	8.74	**8.93**
HOMO–3 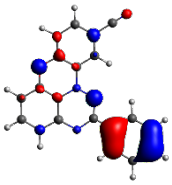	8.768	8.527	8.818	8.84	**8.93**
HOMO–4 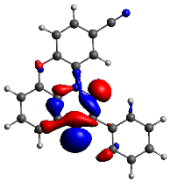	9.211	9.193	9.484	9.50	**9.56**
HOMO–5 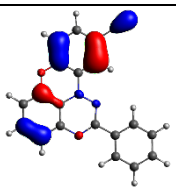	9.270	9.284	9.575	9.59	**9.56**

Table S15. Assignment of experimental ionization energies (IE_n) for radical **1f**. Theoretical values were obtained with the CAM-B3LYP/6-311G(d,p) method. See text for details.

1f 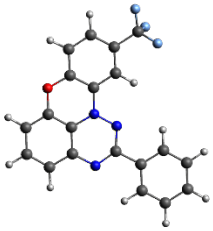 Type of MO	**Method 1** $IE_1 = \Delta E_{SCF}$ $IE_n = \Delta E_{SCF}+E_{TDDFT}$ /eV	**Method 2** $-\varepsilon^{KS}$ /eV	Corrected $-\varepsilon^{KS} + x_{\Delta SCF}$ $x_{\Delta SCF} = 0.304$ /eV	Corrected $-\varepsilon^{KS} + x_{exp}$ $x_{exp} = 0.181$ /eV	Exp. IE /eV
H(S)OMO 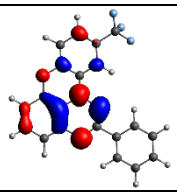	6.683	6.379	6.683	6.56	**6.56**
HOMO–1 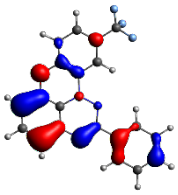	7.601	7.571	7.876	7.75	**8.05**
HOMO–2 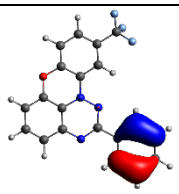	8.636	8.372	8.676	8.55	**8.72**
HOMO–3 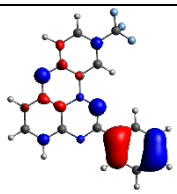	8.697	8.473	8.777	8.65	**8.72**
HOMO–4 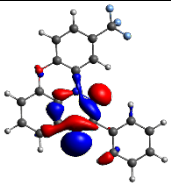	9.150	9.099	9.403	9.28	**9.50**
HOMO–5 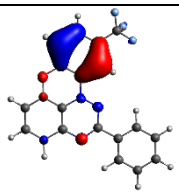	9.210	9.248	9.552	9.43	**9.50**

Table S16. Assignment of experimental ionization energies (IE_n) for radical **1g**. Theoretical values were obtained with the CAM-B3LYP/6-311G(d,p) method. See text for details.

1g 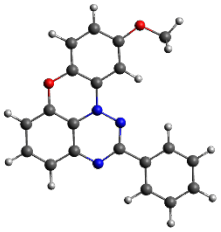 Type of MO	**Method 1** $IE_1 = \Delta E_{SCF}$ $IE_n = \Delta E_{SCF}+E_{TDDFT}$ /eV	**Method 2** $-\varepsilon^{KS}$ /eV	Corrected $-\varepsilon^{KS} + x_{\Delta SCF}$ $x_{\Delta SCF} = 0.305$ /eV	Corrected $-\varepsilon^{KS} + x_{exp}$ $x_{exp} = 0.391$ /eV	Exp. IE /eV
H(S)OMO 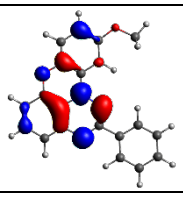	6.364	6.059	6.364	6.45	**6.45**
HOMO–1 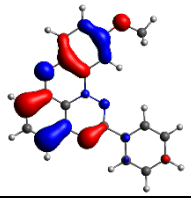	7.058	7.084	7.390	7.48	**7.67**
HOMO–2 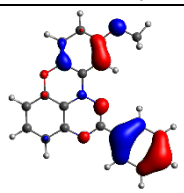	8.309	8.054	8.359	8.45	**8.54**
HOMO–3 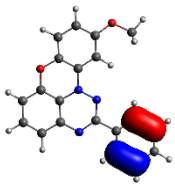	8.365	8.394	8.699	8.785	**8.54**
HOMO–4 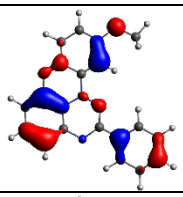	8.798	8.542	8.847	8.93	**9.29**
HOMO–5 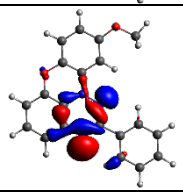	8.960	8.875	9.180	9.27	**9.29**

Table S17. A comparison of experimental and theoretical IE_1.

	IE_1 /eV		
radical	UV-PES	DFT [a]	ΔIE_1 /eV
A	6.40	6.407	0.007
1a	6.45	6.432	-0.018
1b	6.55	6.581	0.031
1c	6.50	6.598	0.098
1d	6.51	6.580	0.070
1e	6.80	6.782	-0.018
1f	6.56	6.683	0.1230
1g	6.45	6.364	-0.086

[a] $IE_1 = \Delta E_{SCF} = E_{SCFcation} - E_{SCFradical}$ at the UCAM-B3LYP/6-311G(d,p).

Graphical correlations of the experimental (UV-PES) and theoretical (DFT) ionization energies listed in Tables S9–S16 are shown in Figure S33. Correlations involving DFT data obtained with methods 2a and 2b have slopes of unity within the error. Therefore, the fitting functions have slopes fixed as 1.0.

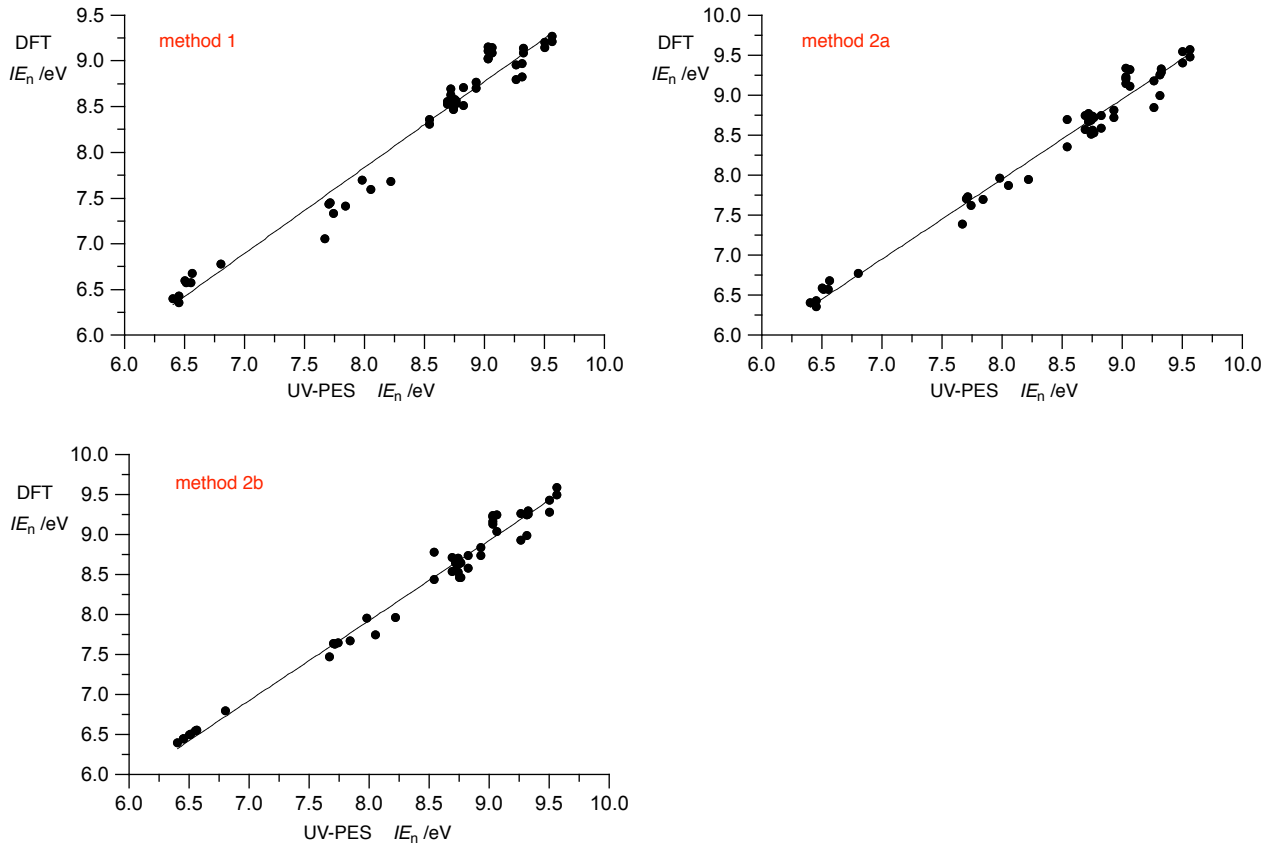

Figure S33. Correlation of ionization energies IE_n obtained for radicals **A** and **1** with UV-PES measurements and DFT calculations using method 1 (as ΔE_{SCF}+$E_{TD\text{-}DFT}$; best-fit function IE_n = 0.32(22)+0.94(3)×IE_n (UVPES), r^2 = 0.965), method 2a (as $-\varepsilon^{KS} + x_{\Delta SCF}$; best-fit function IE_n = -0.042(22)+IE_n (UVPES), r^2 = 0.977), and method 2b (as $-\varepsilon^{KS} + x_{exp}$; best-fit function IE_n (DFT) = -0.07(2)+ IE_n (UVPES), r^2 = 0.980).

d) Electron Affinities (*EA*). Vertical electron affinities (EA_{vert}) for radicals **A** and **1** were calculated as $\Delta E_{SCF} = E_{SCFanion} - E_{SCFradical}$ for fully optimized radical in its ground state and the anion at the radical geometry at the UCAM-B3LYP/6-311++G(d,p)//UCAM-B3LYP/6-311G(d,p) level of theory. Adiabatic electron affinities (EA_{adiab}) for radicals **A** and **1** were calculated as above using $E_{SCFanion}$ energy for fully optimized anion at the UCAM-B3LYP/6-311++G(d,p)//UCAM-B3LYP/6-311G(d,p) level of theory. Results are shown in the summary Table S21.

e) Excitation energies. UV-vis spectra were calculated by using the TD-DFT method[24] at the CAM-B3LYP/6-311++G(d,p)//CAM-B3LYP/6-311G(d,p) level of theory in CH_2Cl_2 dielectric medium. The solvent effect was implemented with the polarizable continuum model (PCM)

using the integral equation formalism (IEFPCM).[25] Both spectra, with and without implicit solvent effect, were calculated for comparison with experimental spectra. Results are shown in Table S18.

Table S18. TD-DFT calculated three lowest energy excitations *E* for **1a**–**1g** with indicated main transitions.[a]

Radical	E_1 /eV, nm	Main contribution	E_2 eV, nm	Main contribution	E_3 /eV, nm	Main contribution
1a	2.353, 526.9	β-HOMO-1 → β-HOMO	2.441, 507.9	α-HOMO → α-LUMO β-HOMO → β-LUMO	3.074, 403.3	α-HOMO → α-LUMO+1
1b	2.328, 532.7	β-HOMO-1 → β-HOMO	2.464 503.1	α-HOMO → α-LUMO	3.065, 404.6	α-HOMO → α-LUMO+1
1c	2.343, 529.2	β-HOMO-1 → β-HOMO	2.460, 504.1	α-HOMO → α-LUMO	3.024, 410.0	α-HOMO → α-LUMO+1
1d	2.345, 528.7	β-HOMO-1 → β-HOMO	2.460, 504.1	α-HOMO → α-LUMO	3.019, 410.7	α-HOMO → α-LUMO+1
1e	2.368, 523.5	β-HOMO-1 → β-HOMO	2.459, 504.3	α-HOMO → α-LUMO β-HOMO → β-LUMO	2.846, 435.6	α-HOMO → α-LUMO+1
1f	2.368, 523.5	β-HOMO-1 → β-HOMO	2.474, 501.1	α-HOMO → α-LUMO	2.991, 414.5	α-HOMO → α-LUMO+1
1g	2.270, 546.1	β-HOMO-1 → β-HOMO	2.419, 512.6	α-HOMO → α-LUMO	3.030, 409.2	α-HOMO → α-LUMO+1

[a] Obtained at the CAM-B3LYP/6-311++G(d,p)//CAM-B3LYP/6-311G(d,p) level of theory in CH_2Cl_2 dielectric medium (IEFPCM).

The TD-DFT calculated excitation energies were correlated with experimental data and results are shown in Figure S34.

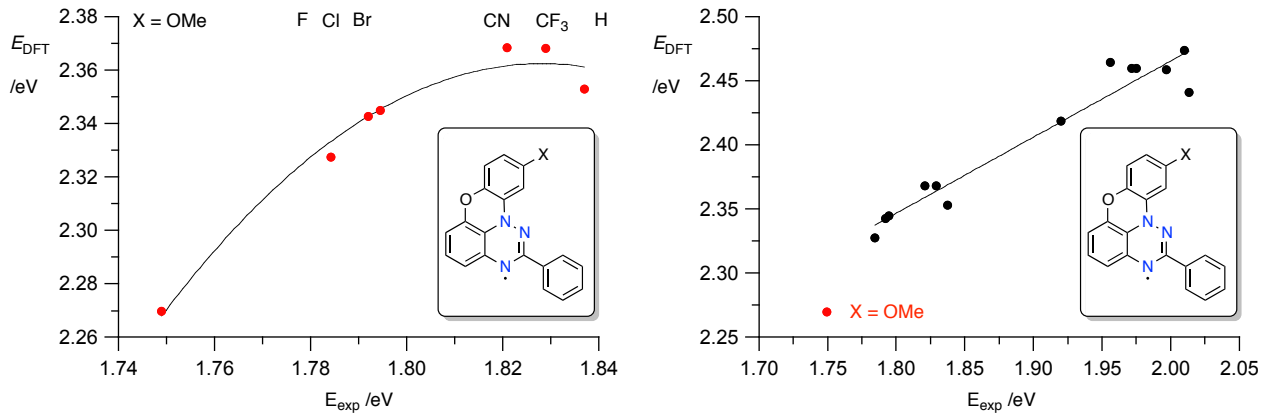

Figure S34. Correlation of experimental (E_{exp}) and DFT calculated (E_{DFT}) excitation energies for radicals **1**. Left: first excitation (lowest energy); right: first and second excitation energies, best-fit function without the red datapoint: E_{DFT} = 1.28(9)+0.59(5)x E_{exp}, r^2 = 0.937.

f) Isotropic Fermi constants (A^{FC}). Isotropic Fermi contact coupling constants (A^{FC}) for radicals **1** were calculated using the UCAM-B3LYP/EPR-III // B3LYP/6-311G(d,p) method in benzene dielectric medium requested with the SCRF(IEFPCM, Solvent=Benzene) keyword (IEFPCM, the default PCM model).[25] The EPR-III[26] is a triple-ζ basis set, which includes diffuse and 2df polarization functions and is optimized for accurate Fermi contact interactions between s-orbitals and the nucleus. Since EPR-III basis set is optimized for elements H–F, for calculations involving **1c** and **1d** containing heavier elements, Cl and Br, respectively, two different basis sets were requested with the *gen* keyword: EPR-III for light elements (H–F), 6-311+G(2df) basis set for the Cl atom and LANL2DZdp basis set and ECP for Br atom. The resulting *hfcc* values are shown in Table S19 and Mulliken spin densities are listed in Table S20.

Table S19. DFT-calculated hyperfine coupling constants (G) for radicals in series **1** in benzene.[a]

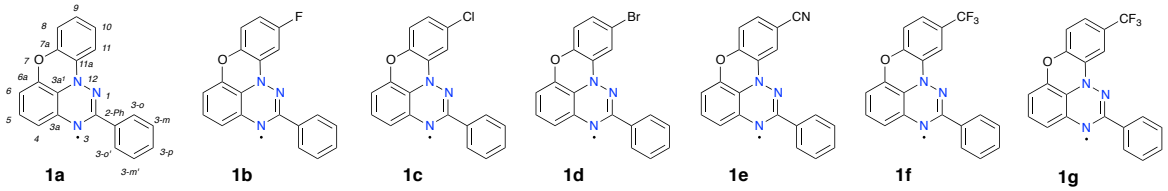

A^{FC} /G	**1a** H	**1b** F	**1c** Cl	**1d** Br	**1e** CN	**1f** CF_3	**1g** OMe
$a_{N(12)}$	6.07	5.78	5.78	5.79	5.59	5.72	6.12
$a_{N(1)}$	3.89	4.02	4.05	4.05	4.20	4.12	3.81
$a_{N(3)}$	4.14	4.17	4.18	4.19	4.25	4.22	4.07
$a_{H(4)}$	-0.44	-0.48	-0.51	-0.52	-0.62	-0.57	-0.35
$a_{H(5)}$	-0.95	-0.86	-0.85	-0.85	-0.78	-0.82	-0.96
$a_{H(6)}$	-0.76	-0.83	-0.87	-0.87	-1.03	-0.95	-0.65
$a_{H(8)}$	0.98	0.97	0.95	0.95	0.86	0.89	1.04
$a_{H(9)}$	-2.33	-2.50	-2.42	-2.40	-2.14	-2.20	-2.74
$a_{H(10)}$	1.05	-	--	-	-	-	-
$a_{H(11)}$	-2.38	-2.32	-2.43	-2.45	-2.60	-2.51	-1.97
$a_{H(2\text{-}o)\ avrg}$	0.49	0.51	0.51	0.51	0.54	0.52	0.47
$a_{H(2\text{-}m)avrg}$	-0.28	-0.30	-0.30	-0.30	-0.31	-0.30	0.28
$a_{H(2\text{-}p)}$	0.40	0.42	0.43	0.43	0.45	0.44	0.39
a_X [b]	-	-2.49	-0.12	0.00	-0.10	-0.95	0.32

[a] CAM-B3LYP/EPR-III // B3LYP/6-311G(d,p) in benzene dielectric medium. [b] *hfcc* (G) for selected atoms at the C(10) position.

Table S20. DFT calculated spin densities for radicals in series **1**.[a]

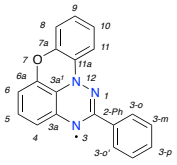

1a

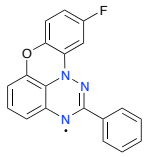

1b

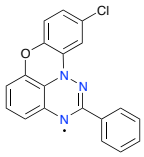

1c

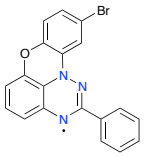

1d

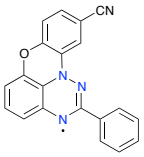

1e

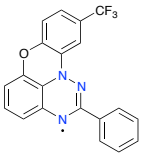

1f

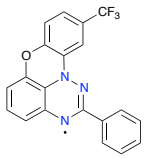

1g

Spin density	**1a** H	**1b** F	**1c** Cl	**1d** Br	**1e** CN	**1f** CF_3	**1g** OMe
$\rho_{N(12)}$	0.242	0.232	0.231	0.233	0.225	0.228	0.240
$\rho_{N(1)}$	0.280	0.287	0.289	0.288	0.299	0.296	0.276
$\rho_{C(2)}$	-0.061	-0.064	-0.059	-0.061	-0.063	-0.060	-0.055
$\rho_{N(3)}$	0.280	0.283	0.284	0.284	0.288	0.285	0.275
$\rho_{C(3a)}$	0.017	0.016	0.014	0.014	0.012	0.015	0.018
$\rho_{C(4)}$	0.003	0.005	0.007	0.007	0.009	0.007	-0.001
$\rho_{C(5)}$	0.032	0.029	0.028	0.028	0.025	0.027	0.032
$\rho_{C(6)}$	0.019	0.022	0.022	0.022	0.029	0.027	0.015
$\rho_{C(6a)}$	0.026	0.021	0.021	0.021	0.017	0.020	0.027
$\rho_{C(3a')}$	0.076	0.081	0.077	0.078	0.077	0.074	0.078
$\rho_{O(7)}$	0.027	0.026	0.026	0.026	0.024	0.025	0.030
$\rho_{C(7a)}$	0.083	0.087	0.085	0.085	0.076	0.077	0.102
$\rho_{C(8)}$	-0.049	-0.048	-0.047	-0.047	-0.040	-0.043	-0.050
$\rho_{C(9)}$	0.086	0.093	0.087	0.086	0.073	0.078	0.099
$\rho_{C(10)}$	-0.046	-0.047	-0.043	-0.045	-0.098	-0.041	-0.044
$\rho_{C(11)}$	0.078	0.074	0.077	0.079	0.083	0.075	0.058
$\rho_{C(11a)}$	-0.065	-0.067	-0.064	-0.066	-0.059	-0.057	-0.068
$\rho_{C(2\text{-}Ph)}$	0.004	0.006	0.006	0.006	0.006	0.005	0.004
$\rho_{C(2\text{-}o)\ avrg}$	-0.020	-0.022	-0.022	-0.021	-0.023	-0.023	-0.020
$\rho_{C(2\text{-}m)\ avrg}$	0.011	0.012	0.011	0.012	0.012	0.012	0.011
$\rho_{C(2\text{-}p)}$	-0.016	-0.017	-0.017	-0.017	-0.018	-0.018	-0.016
ρ_x [c]	-	0.001 (F)	-0.002 (Cl)	-0.002 (Br)	-0.012 (N)	-0.000 (F)	-0.0002 (O)

[a] UCAM-B3LYP/EPR-III // B3LYP/6-311G(d,p) in benzene dielectric medium. Densities on the hydrogen atoms summed to the adjacent carbon atoms. [c] Density of selected atoms at the C(10) position.

The calculated isotropic Fermi contacts A^{FC} values were compared to the experimental *hfcc* and results are shown in Figure S35.

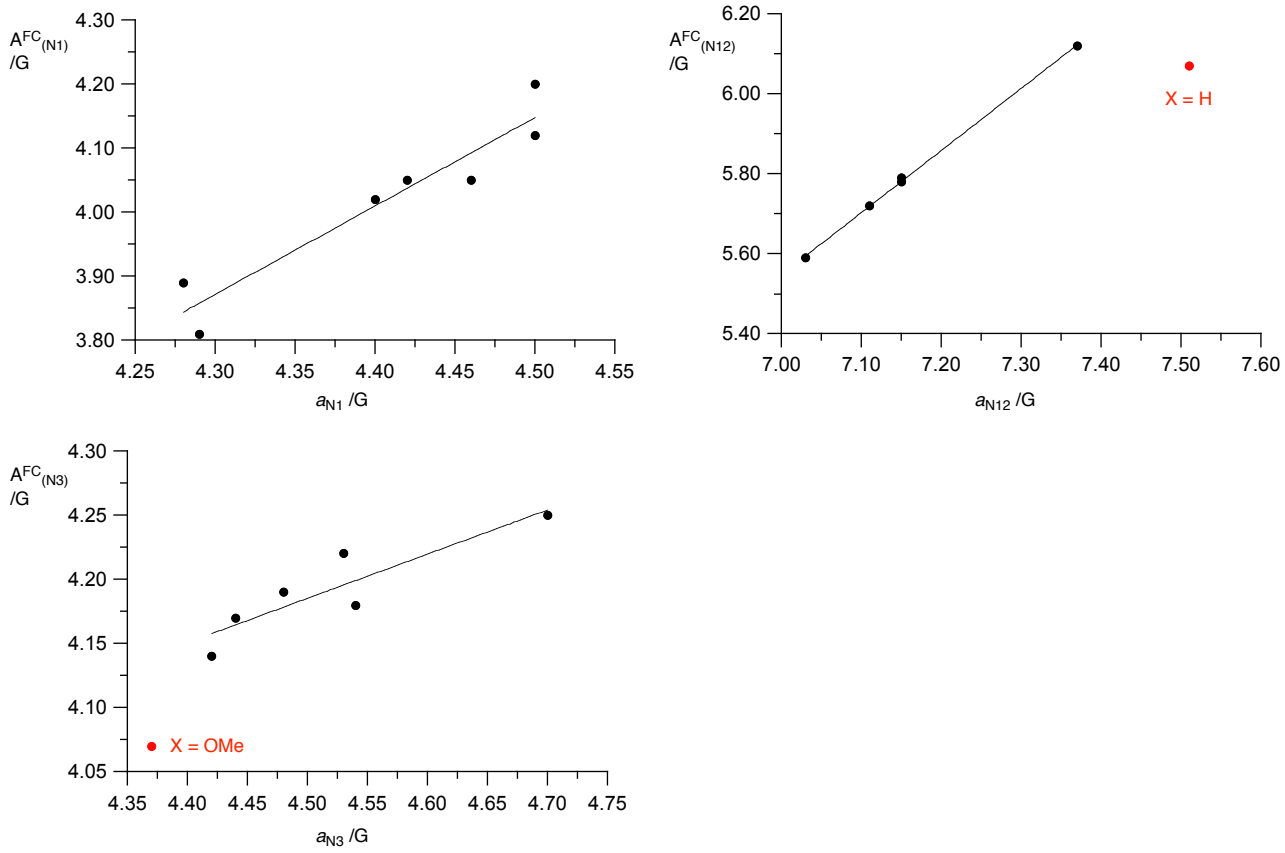

Figure S35. Correlation of experimental *hfcc*, a_N, and DFT derived isotropic Fermi contacts $A^{FC}_{(N)}$ for three N nuclei. Best-fit functions: $A^{FC}_{(N12)} = -5.31(15)+1.55(2) \times a_{N12}$, $r^2 = 0.999$; $A^{FC}_{(N1)} = -2.1(9)+1.38(20) \times a_{N1}$, $r^2 = 0.905$; $A^{FC}_{(N3)} = 2.64(38)+0.34(8) \times a_{N3}$, $r^2 = 0.81$.

g) Spin delocalization. Spin delocalization parameter RDV (Radical Delocalization Value) was calculated according to the formula:[27]

$$RDV = \sum_{i=1}^{n} (\rho_i)^2$$

where Mulliken spin density ρ_i on each heavy atoms *i* (hydrogen atoms summed up to heavy atoms) is obtained with the CAM-B3LYP/EPR-III // CAM-B3LYP/6-311G(d,p) method in benzene dielectric medium using the IEFPCM model[25] [keywords: SCRF(IEFPCM, Solvent=benzene)].

For the purpose of this work, the inverse is reported: $RDV^{-1} = 1/RDV$, since now the larger value corresponds to greater delocalization. Results are shown in Table S21. Spin density maps for all radicals **A** and **1** are shown in Figure S36 and electrostatic potential surface maps in Figure S37.

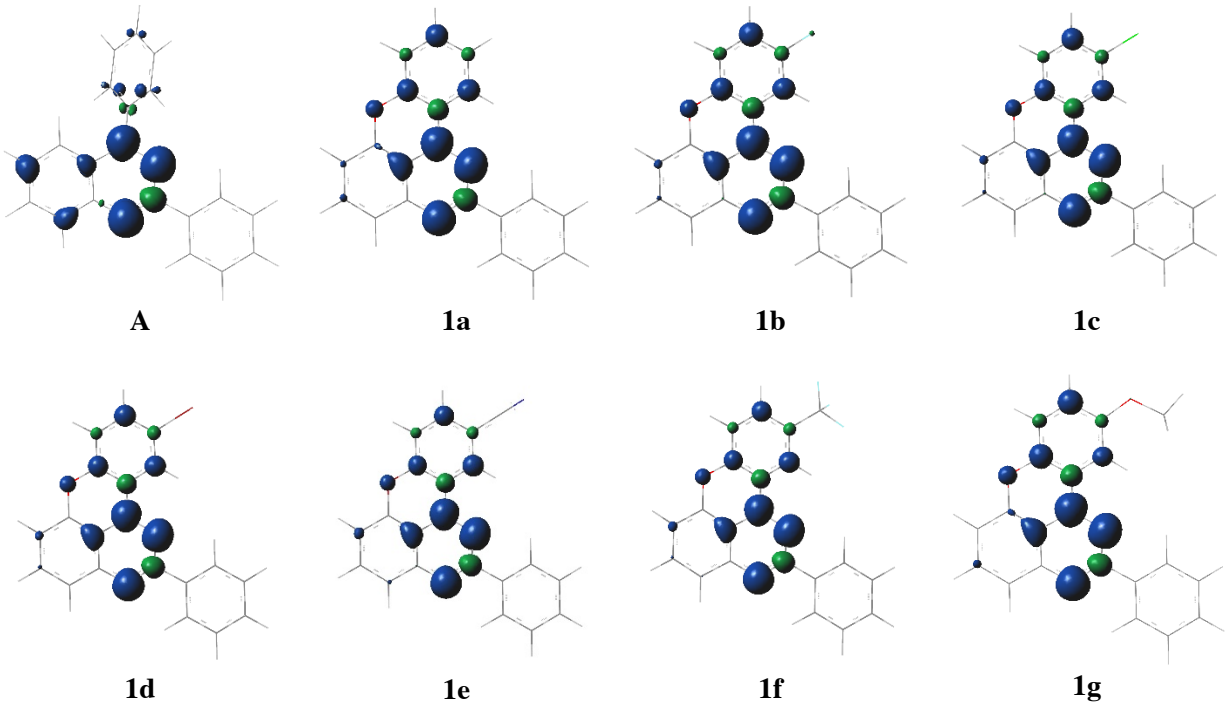

Figure S36. Spin Density Map at the 0.004 electron/bohr^3. UCAM-B3LYP/6 311G(d,p) level of theory.

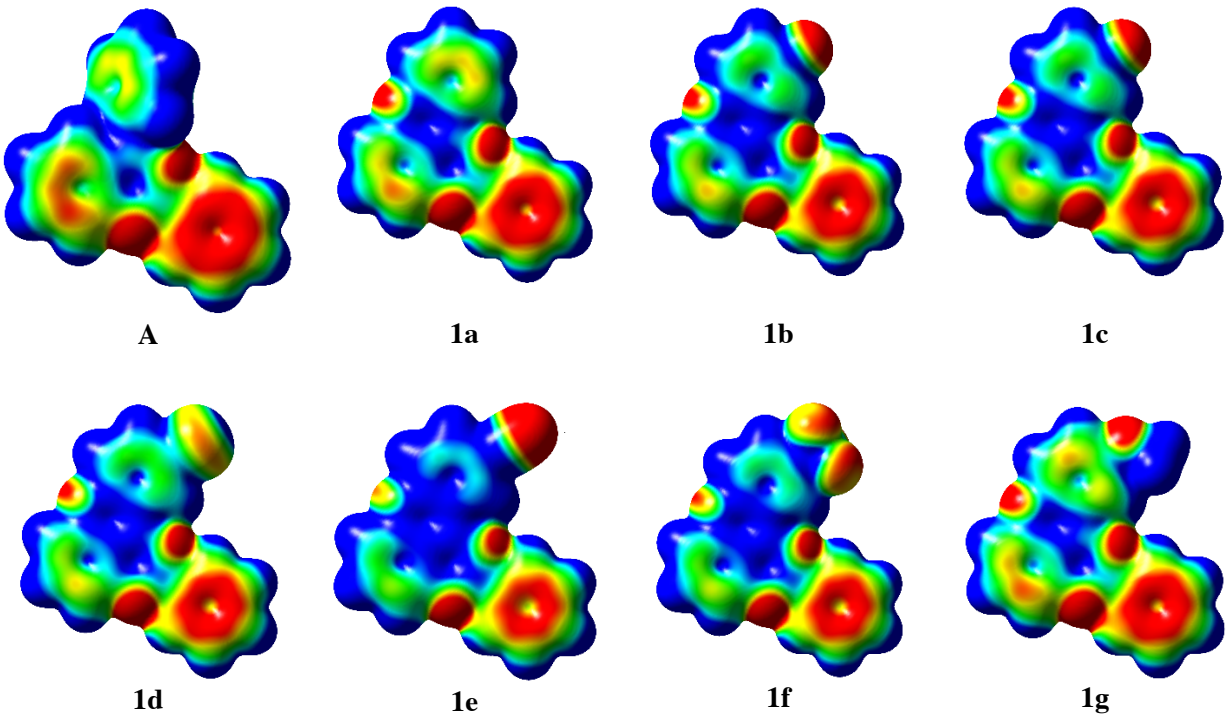

Figure S37. Electrostatic Potential Surface Map at the 0.004 electron/bohr^3 isodensity surface. Electrostatic potential iso-contour level from +12.55 (red) to -12.55 (blue) kcal/mole. UCAM-B3LYP/6 311G(d,p) level of theory.

Table S21. Summary of DFT-derived pertinent molecular parameters for radicals **A** and series **1**.

Radical	**A**	**1a**	**1b**	**1c**	**1d**	**1e**	**1f**	**1g**
ΔE_{SCF} (IE_1) [a] /eV	6.41	6.43	6.58	6.60	6.58	6.78	6.68	6.36
$\varepsilon_{\alpha HOMO}$ [a] /eV	-6.09	-6.11	-6.26	-6.30	-6.29	-6.49	-6.38	-6.06
$\varepsilon_{\alpha LUMO}$ [a] /eV	-0.14	-0.35	-0.45	-0.49	-0.48	-0.77	-0.56	-0.33
$\Delta E_{\alpha HOMO-\alpha LUMO}$ /eV	5.95	5.76	5.81	5.81	5.81	5.72	5.82	5.73
EA_{vert} as ΔE_{SCF} [b] /eV	1.310	1.538	1.707	1.735	1.745	1.933	1.821	1.542
EA_{adiab} as ΔE_{SCF} [c] /eV	1.710	1.717	1.901	1.925	1.935	2.120	2.016	1.732
Δ (IE_1–EA_{vert}) [d] /eV	5.10	4.89	4.87	4.87	4.84	4.85	4.86	4.82
RDV^{-1} [e]	3.612	3.873	3.823	3.841	3.834	3.817	3.863	3.910

[a] $\Delta E_{SCF} = E_{SCFcation} - E_{SCFradical}$; obtained at the UCAM-B3LYP/6-311G(d,p) level theory. See section 9c. [b] Vertical electron affinity $\Delta EA_{vert} = E_{SCFanion} - E_{SCFradical}$ at the CAM-B3LYP/6-311++G(d,p)//CAM-B3LYP/6-311G(d,p); see section 9d. [c] Adiabatic electron affinity $\Delta EA_{adiab} = E_{SCFanion} - E_{SCFradical}$ at the CAM-B3LYP/6-311++G(d,p)//CAM-B3LYP/6-311G(d,p); see section 9d. [d] Difference between ionization energy and electron affinity. [e] obtained at the CAM-B3LYP/EPR-III//CAM-B3LYP/6 311G(d,p) level of theory; see section 9f.

h) Atomic coordinates for CAM-B3LYP/6-311G(d,p) optimized geometry and total energy.

A

C	-1.19295500	1.28996600	-0.06070700
C	-0.06757300	2.13844000	0.02551300
C	1.32171900	0.32150000	0.04510300
H	-3.32519200	1.17622100	-0.33974500
C	-2.47095800	1.82816200	-0.22884700
C	-0.27002700	3.52561300	-0.00258500
C	-1.53511100	4.05117900	-0.13915000
C	-2.63447100	3.19923700	-0.26363000
H	0.60710900	4.15484200	0.07488900
H	-1.67741200	5.12444300	-0.16216100
H	-3.62735800	3.61138200	-0.39401400
N	-0.92838500	-0.07397000	-0.00009000
N	0.33149600	-0.56284700	-0.01653300
N	1.20061100	1.64011200	0.10846400
C	-1.94677000	-1.07415300	0.01253100
C	-1.89148500	-2.10721400	-0.91388600
C	-2.95358200	-1.03848600	0.96896700
C	-2.85957300	-3.09807600	-0.89111300
H	-1.08340600	-2.12688400	-1.63247200
C	-3.92155300	-2.03145500	0.98024200
H	-2.96779200	-0.24706500	1.70722300
C	-3.87918500	-3.06063900	0.05051200
H	-2.81761500	-3.90288000	-1.61476100
H	-4.70392500	-2.00605300	1.72881100
H	-4.63462900	-3.83655000	0.06467800
C	2.69401300	-0.25210900	0.05260400
C	2.89829400	-1.63089200	0.07275200
C	3.79606800	0.59969200	0.04038200
C	4.18434700	-2.14616300	0.07770500
H	2.04019200	-2.28882300	0.08886600
C	5.08109800	0.08080600	0.04528500
H	3.62378400	1.66714400	0.02845000
C	5.27952000	-1.29273900	0.06329200
H	4.33293200	-3.21936800	0.09508600
H	5.93162600	0.75208700	0.03489800
H	6.28472900	-1.69758500	0.06755400

E_{tot}= -896.390940976 au

1a

C	2.68048800	2.86420000	-0.00000400
C	2.37245200	1.52260700	0.00000300
C	1.03917400	1.11876600	0.00000200
C	-0.00798200	2.05006800	-0.00000600
C	0.32153900	3.41256000	-0.00000700
C	1.64362000	3.80170600	-0.00000900
H	3.71990300	3.16329900	-0.00000800
H	-0.48746700	4.13026000	-0.00001400
H	1.89196800	4.85570600	-0.00001000
C	-1.50438800	0.31461700	-0.00000700
C	-2.91154200	-0.16716100	-0.00000500
C	-3.21088900	-1.52851000	-0.00004900
C	-3.95323000	0.75808400	0.00004300
C	-4.52904800	-1.95476000	-0.00004600
H	-2.40236000	-2.24601500	-0.00008700

C	-5.27054600	0.32875300	0.00004900
H	-3.70779100	1.81104300	0.00007400
C	-5.56283600	-1.02810500	0.00000400
H	-4.75091700	-3.01533100	-0.00008500
H	-6.07289700	1.05687700	0.00008600
H	-6.59337400	-1.36318800	0.00000700
C	1.73395100	-1.17872100	0.00000600
C	1.47451600	-2.54423200	0.00001800
C	3.05761500	-0.72783000	0.00000200
C	2.52437000	-3.44711500	0.00002000
H	0.44466200	-2.86811100	0.00002500
C	4.10136300	-1.63330600	0.00000000
C	3.83678300	-2.99454300	0.00001200
H	2.31385300	-4.50886000	0.00002700
H	5.11225300	-1.24709200	-0.00000900
H	4.65862800	-3.69906900	0.00001200
N	0.70350500	-0.22529800	-0.00000200
N	-0.57318300	-0.64298900	0.00000000
N	-1.30634200	1.62448000	-0.00001100
O	3.38665200	0.60433200	-0.00001000

E_{tot}= -970.414588354 au

1b

C	-2.17461300	3.38900600	0.00000700
C	-2.03356700	2.01990500	0.00000600
C	-0.75916700	1.45675400	0.00000300
C	0.39428500	2.25226400	0.00000000
C	0.23410900	3.64488300	0.00000000
C	-1.03043900	4.19241600	0.00000300
H	-3.16940900	3.81349000	0.00000900
H	1.12476500	4.25828500	-0.00000200
H	-1.14815700	5.26882400	0.00000400
C	1.66916700	0.34698100	0.00000100
C	3.00642600	-0.30289200	0.00000100
C	3.13623400	-1.69069700	0.00003700
C	4.15359300	0.48789800	-0.00003400
C	4.39213300	-2.27535600	0.00003800
H	2.24630100	-2.30430800	0.00006600
C	5.40821600	-0.09988400	-0.00003400
H	4.03976500	1.56305800	-0.00006100
C	5.53164400	-1.48234600	0.00000200
H	4.48210800	-3.35505800	0.00006700
H	6.29382000	0.52429700	-0.00006300
H	6.51328900	-1.94122800	0.00000200
C	-1.72413900	-0.73765800	0.00000000
C	-1.62217400	-2.12318600	-0.00000700
C	-2.98481500	-0.13093300	0.00000300
C	-2.78070300	-2.86905400	-0.00001000
H	-0.65159400	-2.59431900	-0.00001000
C	-4.12714800	-0.90762500	0.00000000
C	-4.03539800	-2.29133100	-0.00000700
H	-5.08635400	-0.40730500	0.00000200
H	-4.91678800	-2.91768100	-0.00001000
N	-0.58825300	0.08128000	0.00000300
N	0.62723900	-0.48996200	0.00000300
N	1.63057900	1.67100100	-0.00000300
O	-3.15179300	1.23208400	0.00001000

F	-2.68024800	-4.20842600	-0.00001800

E_{tot}= -1069.65976629 au

1c

C	1.34897700	3.94271200	0.00001400
C	1.46127700	2.57148700	0.00000400
C	0.31311200	1.78291200	-0.00000700
C	-0.96704000	2.35227600	-0.00000800
C	-1.06567500	3.75083900	0.00000000
C	0.07619800	4.52192600	0.00001100
H	2.24864500	4.54305100	0.00002300
H	-2.05399600	4.18985100	-0.00000100
H	-0.00629900	5.60156800	0.00001800
C	-1.86900800	0.24455400	-0.00001900
C	-3.06353400	-0.64043400	-0.00001600
C	-2.93591800	-2.02848900	-0.00005600
C	-4.33655200	-0.07393800	0.00003600
C	-4.06294900	-2.83398700	-0.00004000
H	-1.94857500	-2.46846700	-0.00009700
C	-5.46168900	-0.88231700	0.00005400
H	-4.42241700	1.00382000	0.00006600
C	-5.32880700	-2.26390300	0.00001700
H	-3.95285300	-3.91180500	-0.00006900
H	-6.44695700	-0.43167600	0.00009900
H	-6.20931800	-2.89550400	0.00003200
C	1.66745400	-0.19528300	-0.00000700
C	1.82406200	-1.57547900	-0.00000700
C	2.79353100	0.63414500	0.00000600
C	3.09958000	-2.10789800	0.00000500
H	0.94633300	-2.20230800	-0.00001700
C	4.05883800	0.08040300	0.00001900
C	4.22220500	-1.29601200	0.00001800
H	4.91089700	0.74716100	0.00003000
H	5.21089800	-1.73291600	0.00002800
N	0.39886400	0.39986900	-0.00001600
N	-0.69039800	-0.38574900	-0.00002300
N	-2.07484900	1.55320500	-0.00001400
O	2.70675800	2.00164400	0.00000700
Cl	3.29352300	-3.84284000	0.00000300

E_{tot}= -1430.03762037 au

1d

C	0.66750200	4.40791500	-0.00001500
C	0.04993800	3.17845600	-0.00000500
C	0.81916500	2.01727400	0.00000500
C	2.21932100	2.06580700	0.00000600
C	2.83452700	3.32570500	-0.00000300
C	2.06454200	4.46831400	-0.00001300
H	0.05806600	5.30144800	-0.00002400
H	3.91534600	3.36262600	-0.00000200
H	2.54535500	5.43849000	-0.00002000
C	2.26646000	-0.22620600	0.00001600
C	3.04295700	-1.49396800	0.00001500
C	2.40516500	-2.73341200	0.00004600
C	4.43547200	-1.44524400	-0.00002800
C	3.14881300	-3.90219100	0.00003100

H	1.32491400	-2.77210600	0.00007900
C	5.17629100	-2.61596900	-0.00004400
H	4.91859400	-0.47802500	-0.00005300
C	4.53599100	-3.84744500	-0.00001500
H	2.64326300	-4.86043500	0.00005400
H	6.25862000	-2.56674700	-0.00008100
H	5.11611800	-4.76268400	-0.00002900
C	-1.17781800	0.69031200	0.00000600
C	-1.84053000	-0.53105900	0.00000800
C	-1.91101600	1.88119000	-0.00000500
C	-3.22316400	-0.54739200	-0.00000200
H	-1.25732500	-1.43831100	0.00001600
C	-3.29161000	1.84207600	-0.00001600
C	-3.95938000	0.62699700	-0.00001400
H	-3.83164100	2.77967500	-0.00002600
H	-5.03984500	0.59770300	-0.00002200
N	0.22163500	0.76698300	0.00001300
N	0.93762800	-0.36929700	0.00002000
N	2.94739500	0.91015900	0.00001100
O	-1.31840600	3.11641900	-0.00000700
Br	-4.12647400	-2.21871000	0.00000100

E_{tot}= -3544.05627087 au

1e

C	1.66582600	-3.77559600	0.00000500
C	1.68834800	-2.40108400	0.00000600
C	0.49393600	-1.68635400	0.00000300
C	-0.74721100	-2.33521800	-0.00000100
C	-0.75625400	-3.73778500	-0.00000200
C	0.43181400	-4.43490600	0.00000100
H	2.60184200	-4.31748000	0.00000700
H	-1.71460900	-4.23887400	-0.00000600
H	0.41815300	-5.51749900	0.00000100
C	-1.78114600	-0.28813600	0.00000100
C	-3.02909400	0.51861700	0.00000200
C	-2.99041700	1.91205800	0.00004400
C	-4.26329200	-0.12836400	-0.00003900
C	-4.16653000	2.64387700	0.00004400
H	-2.03391200	2.41553200	0.00007700
C	-5.43761800	0.60653800	-0.00003900
H	-4.28078700	-1.20935700	-0.00007000
C	-5.39318700	1.99382200	0.00000200
H	-4.12541300	3.72643800	0.00007800
H	-6.39205600	0.09390700	-0.00007200
H	-6.31226400	2.56776200	0.00000200
C	1.72086300	0.37325100	0.00000200
C	1.79457400	1.75695300	-0.00000600
C	2.89882700	-0.38495700	0.00000500
C	3.03854200	2.38204500	-0.00000800
H	0.87774800	2.32630300	-0.00000900
C	4.13114900	0.24286700	0.00000200
C	4.20854900	1.62363300	-0.00000400
H	5.01967900	-0.37413200	0.00000500
H	5.17125800	2.11634300	-0.00000600
N	0.49244100	-0.30133700	0.00000500
N	-0.64373300	0.41492300	0.00000500
N	-1.90251800	-1.60770600	-0.00000300

O	2.89717800	-1.74920900	0.00001100
C	3.11273400	3.81160500	-0.00001600
N	3.17816300	4.95805100	-0.00002200

E_{tot}= -1062.63662413 au

1f

C	-0.44922900	4.40561000	-0.01021800
C	0.11656300	3.15223000	-0.00437600
C	-0.69798800	2.02309700	-0.00120600
C	-2.09472900	2.12788600	-0.00445300
C	-2.65834100	3.41203700	-0.01030500
C	-1.84309700	4.52257300	-0.01305800
H	0.19596500	5.27366500	-0.01257000
H	-3.73677900	3.49274900	-0.01277200
H	-2.28418700	5.51136800	-0.01764700
C	-2.23361300	-0.16073800	0.00183900
C	-3.06006700	-1.39609600	0.00216400
C	-2.47207100	-2.65996200	0.00067500
C	-4.44954900	-1.29154700	0.00359400
C	-3.26175900	-3.79808700	0.00068600
H	-1.39424200	-2.74201400	-0.00076800
C	-5.23639400	-2.43179200	0.00374900
H	-4.89382700	-0.30589700	0.00448500
C	-4.64561500	-3.68781500	0.00228200
H	-2.79484900	-4.77568700	-0.00060100
H	-6.31588600	-2.33951800	0.00495000
H	-5.26186000	-4.57912000	0.00230000
C	1.24450800	0.61741600	0.01063900
C	1.86180300	-0.62466800	0.02511400
C	2.02572900	1.77899400	0.00780800
C	3.24503700	-0.70234000	0.03477000
H	1.24542900	-1.51052200	0.03765200
C	3.40501900	1.68960100	0.01969300
C	4.02010600	0.44925900	0.03226300
H	3.97766500	2.60738500	0.02214800
H	5.09890900	0.37701800	0.04961600
N	-0.15095600	0.75054700	0.00496000
N	-0.91128500	-0.35652600	0.00581800
N	-2.86818900	1.00246000	-0.00243100
O	1.48337100	3.03338600	-0.00201700
C	3.90632900	-2.04623400	-0.00611900
F	4.12225800	-2.45678800	-1.26879300
F	5.10216000	-2.03210200	0.60505900
F	3.16156600	-2.99204600	0.58680700

E_{tot}= -1307.47924387 au

1g

C	1.68559600	3.84777600	-0.00000600
C	1.70293900	2.47039200	-0.00001000
C	0.50046900	1.76516400	-0.00000500
C	-0.73619900	2.42491600	0.00000300
C	-0.73623300	3.82606300	0.00000700
C	0.45796700	4.51479200	0.00000200
H	2.62559800	4.38278400	-0.00001000

H	-1.69112000	4.33373700	0.00001300
H	0.45162800	5.59768800	0.00000400
C	-1.78504800	0.38766900	-0.00000300
C	-3.04138300	-0.40923900	-0.00000400
C	-3.01624900	-1.80274800	-0.00006700
C	-4.27003000	0.24771900	0.00005700
C	-4.19882100	-2.52447300	-0.00006800
H	-2.06279100	-2.31213800	-0.00011700
C	-5.45123200	-0.47654700	0.00005700
H	-4.27619100	1.32887400	0.00010300
C	-5.41999400	-1.86412200	-0.00000500
H	-4.16799600	-3.60761500	-0.00011900
H	-6.40095600	0.04496600	0.00010700
H	-6.34428600	-2.42975800	-0.00000500
C	1.71240700	-0.30463800	-0.00000400
C	1.76193100	-1.69729900	0.00000700
C	2.88795200	0.44184200	-0.00000900
C	2.99196300	-2.33637600	0.00001200
H	0.82560800	-2.23039400	0.00001200
C	4.11082900	-0.20761600	-0.00000400
C	4.16979200	-1.58598900	0.00000600
H	5.01041200	0.39393900	-0.00000800
H	5.11684200	-2.10836600	0.00001000
N	0.48806100	0.37861100	-0.00000800
N	-0.65585400	-0.32621300	-0.00000900
N	-1.89911700	1.70659800	0.00000600
O	2.90197600	1.81786300	-0.00001900
O	3.14753400	-3.68217100	0.00002300
C	1.98768400	-4.49064800	0.00003100
H	1.37974000	-4.31632300	-0.89313500
H	1.37974100	-4.31630800	0.89319300
H	2.34001900	-5.51942100	0.00003900

E_{tot}= -1084.92268052 au

10. References

[1] P. Bartos, B. Anand, A. Pietrzak, P. Kaszyński, *Org. Lett.* **2020**, *22*, 180-184.

[2] P. Kaszynski, C. P. Constantinides, V. G. Young, Jr., *Angew. Chem. Int. Ed.* **2016**, *55*, 11149 –11152.

[3] Agilent (2014). CrysAlis PRO. Agilent Technologies Ltd, Yarnton, Oxfordshire, England.

[4] G. M. Sheldrick, *Acta Cryst., Sect. A* **2015**, *A71*, 3-8.

[5] G. M. Sheldrick, *Acta Cryst., Sect. C* **2015**, *C71*, 3-8.

[6] N. G. Connelly, W. E. Geiger, *Chem. Rev.* **1996**, *96*, 877–910.

[7] L. E. Lyons, *Aust. J. Chem.* **1980**, *33*, 1717 - 1725.

[8] W. Schmidt, *J. Chem. Phys.* **1977**, *66*, 828-845.

[9] J. Sworakowski, J. Lipinski, K. Janus, *Org. Electron.* **2016**, *33*, 300-310.

[10] a) E. Clar, W. Schmidt, *Tetrahedron* **1977**, *33*, 2093–2097; b) E. Clar, W. Schmidt, *Tetrahedron* **1979**, *35*, 1027-1032.

[11] A. P. Davis, A. J. Fry, *J. Phys. Chem. A* **2010**, *114*, 12299–12304.
[12] P. I. Djurovich, E. I. Mayo, S. R. Forrest, M. E. Thompson, *Org. Electron.* **2009**, *10*, 515–520.
[13] R. S. Ruoff, K. M. Kadish, P. Boulas, E. C. M. Chen, *J. Phys. Chem.* **1995**, *99*, 8843-8850.
[14] J. Sworakowski, *Synth. Metals* **2018**, *235*, 125-130.
[15] Gaussian 09, Revision D.01. M. J. Frisch, G. W. Trucks, H. B. Schlegel, G. E. Scuseria, M. A. Robb, J. R. Cheeseman, G. Scalmani, V. Barone, B. Mennucci, G. A. Petersson, H. Nakatsuji, M. Caricato, X. Li, H. P. Hratchian, A. F. Izmaylov, J. Bloino, G. Zheng, J. L. Sonnenberg, M. Hada, M. Ehara, K. Toyota, R. Fukuda, J. Hasegawa, M. Ishida, T. Nakajima, Y. Honda, O. Kitao, H. Nakai, T. Vreven, J. A. Montgomery, Jr., J. E. Peralta, F. Ogliaro, M. Bearpark, J. J. Heyd, E. Brothers, K. N. Kudin, V. N. Staroverov, T. Keith, R. Kobayashi, J. Normand, K. Raghavachari, A. Rendell, J. C. Burant, S. S. Iyengar, J. Tomasi, M. Cossi, N. Rega, J. M. Millam, M. Klene, J. E. Knox, J. B. Cross, V. Bakken, C. Adamo, J. Jaramillo, R. Gomperts, R. E. Stratmann, O. Yazyev, A. J. Austin, R. Cammi, C. Pomelli, J. W. Ochterski, R. L. Martin, K. Morokuma, V. G. Zakrzewski, G. A. Voth, P. Salvador, J. J. Dannenberg, S. Dapprich, A. D. Daniels, O. Farkas, J. B. Foresman, J. V. Ortiz, J. Cioslowski, and D. J. Fox. Gaussian, Inc., Wallingford CT, 2013. Gaussian, Inc., Wallingford CT 2013.
[16] a) A. D. Becke, *Phys. Rev. A* **1988**, *38*, 3098–3100; b) A. D. Becke, *J. Chem. Phys.* **1993**, *98*, 5648–5652; c) C. Lee, W. Yang, R. G. Parr, *Phys. Rev. B* **1988**, *37*, 785–789; d) T. Yanai, D. P. Tew, N. C. Handy, *Chem. Phys. Lett.* **2004**, *393*, 51–57.
[17] R. Krishnan, J. S. Binkley, R. Seeger, J. A. Pople, *J. Chem. Phys.* **1980**, *72*, 650–654.
[18] a) M. D. Hanwell, D. E. Curtis, D. C. Lonie, T. Vandermeersch, E. Zurek, G. R. Hutchison, *J. Chemoinform.* **2012**, *4*, 1–17; b) Avogadro: An Open-Source Molecular Builder and Visualization Tool. Version 1.2.0. Http://Avogadro.Cc/.
[19] a) R. Bartnik, P. Baylère, A. Chrostowska, A. Galindo, S. Leśniak, G. Pfister-Guillouzo, *Eur. J. Org. Chem.* **2003**, *2003*, 2475-2479; b) A. Chrostowska, A. Matrane, D. Maki, S. Khayar, H. Ushiki, A. Graciaa, L. Belachemi, J.-C. Guillemin, *ChemPhysChem* **2012**, *13*, 226-236; c) T. Y. Vu, A. Chrostowska, T. K. X. Huynh, S. Khayar, A. Dargelos, K. Justyna, B. Pasternak, S. Leśniak, C. Wentrup, *Chem. Eur. J.* **2013**, *19*, 14983-14988.
[20] a) V. Lemierre, A. Chrostowska, A. Dargelos, C. H., *J. Phys. Chem. A* **2005**, *109*, 8348–8355; b) R. E. Stratmann, G. E. Scuseria, M. J. Frisch, *J. Chem. Phys.* **1998**, *109*, 8218-8224; c) M. E. Casida, C. Jamorski, K. C. Casida, D. R. Salahub, *J. Chem. Phys.* **1998**, *108*, 4439–4449.
[21] T. Koopmans, *Physica* **1934**, *1*, 104-113.
[22] R. Stowasser, R. Hoffmann, *J. Am. Chem. Soc.* **1999**, *121*, 3414–3420.
[23] A. Mazière, A. Chrostowska, C. Darrigan, A. Dargelos, A. Graciaa, H. Chermette, *J. Chem. Phys.* **2017**, *147*, 164306.
[24] R. E. Stratmann, G. E. Scuseria, M. J. Frisch, *J. Chem. Phys.* **1998**, *109*, 8218-8224.

[25] a) M. Cossi, G. Scalmani, N. Rega, V. Barone, *J. Chem. Phys.* **2002**, *117*, 43-54, and references therein; b) V. Barone, M. Cossi, J. Tomasi, *J. Chem. Phys.* **1997**, *107*, 3210-3221.

[26] a) V. Barone, in *Recent Advances in Density Functional Methods, Vol. 1* (Ed.: D. P. Chong), World Scientific Publ. Co., Singapore, **1996**, pp. 287-334; b) N. Rega, M. Cossi, V. Barone, *J. Chem. Phys.* **1996**, *105*, 11060–11067.

[27] F. De Vleeschouwer, A. Chankisjijev, W. Yang, P. Geerlings, F. De Proft, *J. Org. Chem.* **2013**, *78*, 3151-3158.